Environmental Science
Nano

CRITICAL REVIEW

Hicham Meskher, Soumya Kanti Hazra, Md. Shamim Ahamed,
Iseult Lynch *et al.*
Recent advances in applications of MXenes for desalination,
water purification and as an antibacterial: a review

ROYAL SOCIETY
OF **CHEMISTRY**

CRITICAL REVIEW

Check for updates

Recent advances in applications of MXenes for desalination, water purification and as an antibacterial: a review

Hicham Meskher, [iD] *[ai] Amrit Kumar Thakur, [iD] [bj] Soumya Kanti Hazra,*[c] Md. Shamim Ahamed,*[b] Ahmed Mortuza Saleque, [iD] [d] Qusay F. Alsalhy,[e] Muhammad Wakil Shahzad,[f] Md. Nahian Al Subri Ivan,[g] Shuvra Saha[g] and Iseult Lynch [iD] *[h]

Membranes have become a basis in tackling the global challenge of freshwater scarcity, notably in the fields of desalination and water purification. MXenes, distinguished by their notable high aspect ratio, extensive surface area, robust mechanical strength, and enduring chemical resilience, have emerged as highly promising materials for membrane development. Recent progress in the research and application of MXene membranes, especially in the areas of water desalination and treatment, marks a significant leap forward in this domain. This study conducts an exhaustive analysis of the state-of-the-art developments in the creation and enhancement of MXene-based membranes. It delves into their application in various desalination processes, including membrane-based desalination and solar-driven interfacial steam generation, alongside their use in water purification. This analysis sheds light on their efficacy in desalination processes, in addition to evaluating their antimicrobial properties and salt rejection efficiency. Moreover, the review provides an in-depth examination of the mechanics behind MXene membranes and assesses their overall impact, pinpointing both the current opportunities they present and the challenges they face. The primary goal of this discussion is to enrich the collective understanding of MXene membrane technology and to drive continuous improvement and innovation in this area. By doing so, it aims to contribute to the advancement of sustainable solutions to water scarcity through the development of more efficient and effective membrane technologies.

Environmental significance

Wastewater purification is a critical aspect in protecting the environment from toxic and hazardous materials, requiring efficient wastewater purification membranes. Unfortunately, most wastewater purification methods rely on sophisticated systems that require huge energy consumption, expensive maintenance, and suffer from various drawbacks such as fouling, permeability decrease and selectivity-related issues. To overcome these limitations, improved water purification and desalination systems are using advanced membranes containing exceptional materials such as MXenes. The present study highlights the key features of MXenes and their applications to prepare high performance membranes for desalination, utilising MXenes' fouling resistance and their antibacterial activity. The review aims to explore opportunities to widen the environmental application of MXene-based-membranes including reducing costs, and increasing scalability, stability and membrane reusability.

1. Introduction

Recent advances in the application of MXenes for desalination, water purification, and antibacterial uses have gained considerable momentum, largely driven by the growing global issue of water scarcity.[1,2] The need for efficient and sustainable desalination methods has become more urgent than ever.

[a] Division of Process Engineering, College of Science and Technology, Chadli Bendjedid University, 36000, Algeria. E-mail: h.meskher@univ-eltarf.dz

[b] Department of Biological and Agricultural Engineering, University of California, Davis, CA, USA. E-mail: mahamed@ucdavis.edu

[c] Department of Mechanical Engineering, Indian Institute of Technology Patna, Patna 801103, Bihar, India. E-mail: soumyakantihazra@gmail.com

[d] Department of Electrical and Computer Engineering, University of California, Davis, CA 95616, USA

[e] Membrane Technology Research Unit, Department of Chemical Engineering, University of Technology-Iraq, Alsinaa Street 52, Baghdad 10066, Iraq

[f] Mechanical and Construction Engineering Department, Northumbria University,

Newcastle Upon Tyne, UK

[g] Department of Applied Physics and Materials Research Center, The Hong Kong Polytechnic University, Hung Hom, Kowloon, Hong Kong

[h] School of Geography, Earth and Environmental Sciences, University of Birmingham, Edgbaston, B15 2TT Birmingham, UK. E-mail: i.lynch@bham.ac.uk

[i] GuangDong Engineering Technology Research Center of Advanced Polymer Synthesis, Key Laboratory for Preparation and Application of Ordered Structural Materials of Guangdong Province, College of Chemistry and Chemical Engineering, Shantou University, Guangdong 515063, China

[j] Department of Mechanical Engineering, KPR Institute of Engineering and Technology, Arasur, Coimbatore 641407, Tamil Nadu, India

Among the various water purification techniques, membrane-based processes are receiving significant attention from both researchers and policymakers due to several advantages that they offer.[3,4] These include the exceptional properties of membranes, their ease of maintenance, compact modular design,[5] and the minimal chemical sludge produced during treatment processes.[6,7] However, a persistent challenge with membrane technology is fouling, which leads to reduced permeability and issues related to selectivity.[8–10] Fouling results in higher transmembrane pressure, which in turn limits the membrane's permeability, reduces its lifespan, and ultimately diminishes the overall efficiency of desalination and water purification systems.[8,11] To counteract these limitations, researchers have begun exploring the use of advanced nanostructured materials[12] such as zeolites,[13] metal–organic frameworks (MOFs),[14] and carbon-based materials to reduce fouling.[15] These materials have distinct nanostructures that improve the desalination efficiency by offering better surface properties, separation performance, and hydrophilicity. Among these novel materials, MXenes have emerged as a promising class of two-dimensional (2D) inorganic compounds for water treatment applications.

Produced through a range of different synthesis procedures, MXenes are unique materials composed of transition metal carbides, nitrides, or carbonitrides, which feature metallic conductivity and hydrophilic surfaces terminated with hydroxyl or oxygen groups (Fig. 1). This combination of properties makes MXenes highly attractive for water purification.[16–18] They possess several key characteristics that are ideal for water desalination and purification, including a large surface area, ease of surface functionalization, impressive antifouling properties, robust mechanical strength, and exceptional sieving and water

transport capabilities.[19–23] Ding et al.[24] highlighted MXenes' ability to swell in water and delaminate rapidly, due to electrostatic forces and hydrogen bonding, which significantly enhances membrane performance and separation accuracy. To date, titanium-based MXenes (such as $Ti_3C_2T_x$) have shown the greatest potential for environmental applications. This is primarily due to the abundance of raw titanium in the environment and its non-toxic nature, making it a safe and generally sustainable option for large-scale applications. The innovation surrounding MXene-based membranes has been substantial, with numerous experimental and theoretical studies highlighting their ability to remove ions of varying sizes and charges through their nanoscale channel structures.[25,26] However, producing vertically aligned MXene membranes on a large scale has proven difficult.[27–29] The current research has largely focused on simulations of MXene nanochannels due to the complexities involved in scaling up these materials for industrial use. To enable widespread commercial adoption of MXene membranes, it is crucial to develop more efficient and cost-effective manufacturing processes. Although MXene membranes exhibit outstanding separation properties, challenges remain in scaling up production to achieve large membrane areas with minimal defects, which are necessary for practical desalination applications. Therefore, future research should focus on optimizing interlayer spacing and pore sizes to produce MXene-based membranes at an industrial scale.

MXenes can also be incorporated into other membrane systems, such as polyamide (PA) membranes, to further improve desalination performance.[31,32] The introduction of MXenes into PA membranes results in composite MXene membranes that exhibit enhanced stability and chlorine resistance, which is crucial for long-term desalination applications. MXenes prevent
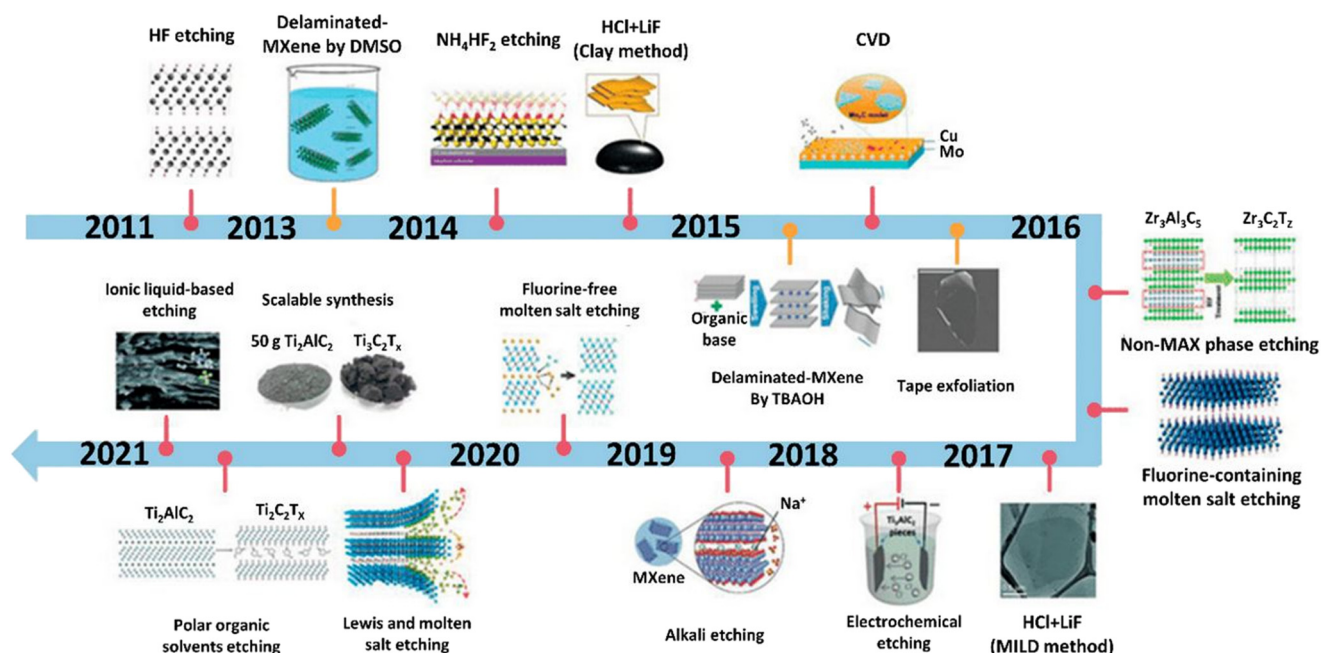

Fig. 1 Advancements in the synthesis of MXene through various approaches. Reproduced from ref. 30 with permission from Wiley, copyright 2021.

the reaction between PA membranes and chlorine,[32,33] significantly extending the lifespan and efficiency of the membranes. Additionally, the integration of MXenes into these membranes introduces new physical and chemical properties that enhance water purification efficiency by improving factors such as membrane durability, fouling resistance, and ion rejection performance.[34–36]

MXenes have also garnered significant interest due to their rich surface functional groups, high electrical conductivity, and excellent dispersibility, positioning them as efficient materials for energy storage applications. Nevertheless, their propensity to restack through van der Waals forces can limit ionic kinetics and reduce the availability of active sites, thereby impacting their overall performance. Transitioning from 2D MXenes into 3D structures presents a promising solution to these challenges, enhancing porosity, surface area, and ion transport. Bashir et al.,[37] have explored innovative methods for fabricating 3D MXene architectures, highlighting their potential applications in advanced energy storage devices across various metal-ion batteries. Similarly, Zhao et al.,[38] investigated MXene/CoO composites as electrocatalysts in vanadium redox flow batteries, demonstrating a 23% increase in energy efficiency when employing MXene composite-modified graphite felt electrodes. This improvement is attributed to the increased active sites and enhanced redox kinetics facilitated by the MXene composite. Additionally, MXene–polypyrrole nanocomposites are emerging as promising candidates for energy storage electrodes. Ezika et al.,[39] utilized density functional theory to identify these nanocomposites as viable anode materials for sodium-ion batteries. Saeed et al.,[40] demonstrated that heterostructures combining metal sulfides and MXenes can enhance electrochemical performance, achieving a high Li-ion storage capacity of 700 mA h g^{-1} with stable cycling. Moreover, Xu et al.[41] developed MXene-based electrodes that significantly improved lithium-ion battery performance, achieving a specific capacity of 1030 mA h g^{-1} after 150 cycles. Density functional theory calculations further revealed strong Li$^+$ adsorption and improved ion kinetics. Lastly, Teenakul et al.,[42] addressed the challenge of competing reactions in vanadium redox flow batteries by coating carbon electrodes with MXene. Their flow battery tests at 130 mA cm^{-2} demonstrated stable discharge capacity over 100 cycles, along with improved voltage and energy efficiency compared to untreated electrodes. Collectively, these studies underscore the significant potential of MXene coatings to enhance electrocatalytic activity and overall battery performance in vanadium redox flow batteries.

MXene membranes show exceptional potential in separating a wide range of ions based on their charge and hydration.[28,43,44] By placing MXene laminates on polymeric substrates, researchers have been able to optimize the membranes' efficiency and separation performance. For molecules larger than 2.5 nm, MXene membranes based on anodic aluminium oxide substrates have demonstrated remarkable separation capabilities.[45,46] Further studies[47–52] have shown that MXene-based membranes exhibit high flux

and excellent salt rejection properties, making them highly effective for desalination. MXenes treated with silver nanoparticles have also displayed impressive antibacterial,[53] antifouling,[47,54] and dye removal characteristics,[55] further enhancing their suitability for water treatment applications. A comprehensive review by Dixit et al.,[21] explored the broad range of MXene applications in water treatment and desalination, highlighting their diverse properties and the many ways they can be used in processes such as adsorption and photocatalysis. While the review focused primarily on water treatment, it also touched on desalination methods such as electrochemical treatments and solar thermal desalination. Despite the progress, there is still a need for more in-depth exploration of MXenes' potential in desalination processes. Zhou et al.[56] delved into MXenes' role in interfacial solar steam generation for desalination, examining the photothermal conversion behaviour of MXenes, the dynamics of water transport, and salt resistance, all of which contribute to the efficiency of solar desalination.

However, significant gaps remain in the current literature. For instance, there is a lack of a comprehensive timeline that outlines the development of MXenes and their potential applications in desalination. Additionally, key challenges, such as the scalability of MXene membranes and their implementation in regions lacking centralized water infrastructure, need further investigation. Much of the existing research focuses on specific desalination techniques, which limits the broader understanding of MXenes' versatility across various approaches. This review aims to address these gaps by providing a comprehensive overview of MXenes' applicability across diverse desalination methods. It highlights the main parameters that make MXenes ideal for water desalination and purification, including their demonstrated antibacterial properties. The review also presents a detailed timeline depicting the evolution of MXene-based technologies, as well as a summary of their potential applications in membrane-based water desalination. Additionally, it discusses solar-driven interfacial steam generation as an alternative desalination technique, with a focus on MXene-based advances in this area, especially their salt rejection capabilities. Finally, the review outlines the key challenges that must be overcome to facilitate the widespread use of MXenes in desalination, including addressing issues related to cost, scalability, stability, repeatability, and the development of cleaner synthesis routes to reduce their environmental impact.

2. MXene membranes for water desalination

MXenes have piqued the interest of researchers working on novel membranes for water desalination because of their exceptionally long graphitic channels of nanoscale diameter.[34] MXenes-based membranes are classified into two categories: freestanding and composite MXenes.[30] Compared to old desalination membranes, such as reverse osmosis and thin-film composite (TFC), MXenes-based membranes have

1014 | *Environ. Sci.: Nano*, 2025, **12**, 1012–1036

This journal is © The Royal Society of Chemistry 2025

exhibited excellent performance and.[57,58] MXenes can also improve fouling resistance, desalination performance, water flow, and other membrane functionalities because they contain nanochannels that let molecules pass through for "molecular-sieving", which improves the selectivity of the prepared membrane to separate the selected molecules.[47,59] Another advantage of composite MXene membranes over vertically aligned (VA) MXene membranes is their ease of manufacture and large-scale application.[60–62] Next, we present the synthesis routes of MXenes and the factors that influence desalination.

2.1 MXenes synthesis approaches

The synthesis technique or route used in producing MXenes substantially affects the resulting material's physicochemical properties and the fields of application in which it can be utilized. Generally, two main types of MXene synthesis methods can be defined: top-down (etching) and bottom-up methods.[63–65] However, the top-down synthesis procedure is considered the most widely used approach to producing MXenes. In addition, there are numerous manufacturing methods for top-down synthesis techniques, such as solution processing, sonication, mechanical force, or selective etching of bulk material. With top-down methods, the materials are typically created in a less uniform way with a distribution in the particle size, defect density, and consequently, characteristics. Top-down strategies benefit from conventional chemical engineering procedures. There aren't many new obstacles to be overcome, and they are easily scalable using present technologies, making them less expensive and more suitable for large-scale production.[66] Most MXene synthesis reports follow a common method, involving the utilization of MAX phases, which are polycrystalline nanolaminates of ternary carbides and nitrides. These MAX phases are denoted by their general formula $M_{n+1}AX_n$, where M represents a transition metal, A is an A-group element (typically IIIA and IVA, e.g., Al, Si, and Ga), X denotes C and/or N, and n ranges from 1 to 3. The synthesis process entails the removal of the "A" atom from the middle layer using various methods. Recent research introduced new fabrication routes, including etching of non-MAX phases or using alternative A-element carbide layers.[54] During the early phase of MXene synthesis, fluorine-containing compounds like HF (hydrofluoric acid) dominated the process (HF in 2011, LiF + HCl in 2014, bifluoride salts in 2014, and molten salt in 2016). However, recent advances have introduced electrochemical etching as a safer alternative, eliminating the need for hazardous HF and allowing better control over MXene surface properties.[63] Electrochemical fluoride-free MXene synthesis using binary aqueous systems, reported in 2018, marked a significant step in reducing safety risks associated with MXene production. Furthermore, molten salt etching, introduced in 2019–2020, has emerged as a more scalable approach, producing MXenes without the need for fluoride-based etchants.[62] The synthetic

methods vary based on the required physical and chemical properties, such as defect density, lateral flake size, and surface functionality. Etching agents play a crucial role, as this choice impacts surface chemistry, hydrophilic properties, oxidation sensitivity, conductivity, and flake size.[67] Notable techniques include HF etching,[68] alkali etching,[69] halogen etching,[70] and Lewis acid molten salt etching,[71] each producing MXenes for different applications. However, the long etching times and hazardous solutions used in traditional HF methods present significant challenges. Recent advances include improvements in surface functionalization, which significantly enhance MXene oxidation stability. The addition of antioxidant agents during synthesis has been shown to mitigate oxidation and increase MXene membrane lifespan in aqueous environments, which is crucial for desalination applications.[68]

The HF etching synthetic method is used to obtain MXenes for electromagnetic and electronic applications,[72] for mechanical applications,[73] and for environmental and sensing applications comprising trace metal adsorption, chemical (liquid, gas) and membranes (gas and liquid) separation.[74] Note that for those fields of applications, there are other possible synthetic methods to produce MXenes, including alkali etching and halogen etching.[65] In recent years, newly developed MXene systems incorporating transition metals such as molybdenum (Mo), vanadium (V), and niobium (Nb) have exhibited unique characteristics and applications.[17] Mo-based MXene is also the first and only success utilizing CVD as the synthetic method, whereas V-based MXenes (e.g., V_2CT_x and $V_4C_3T_x$) can be generated by a variety of top-down approaches.[19] For V-based MXenes, for example, the HF etching approach and the fluoride salt + HCl etching method remain two of the most effective procedures.[22] However, the lengthy etching time and highly poisonous solution are the key obstacles where synthetic technique advancement is desired for safe and cost-effective synthesis techniques to prepare MXenes with desired functionalities.[20] To date, layered Nb_2CT_x MXene may be created using three different etching methods: HF etching, LiF + HCl etching (HF-forming), and hydrothermal.[58]

The success of synthesizing a new MAX phase, innovation in the synthesis approach, and new understanding of the synthetic method are all required for the discovery of new-MXene. Top-down tactics, such as various etching procedures, continue to dominate because of their ability to produce high-quality MXenes. Because of their excellent etching effect, HF and HF-forming (LiF + HCl) procedures are extensively used among these top-down strategies. However, for safety and environmental reasons, the development of non-HF methods such as the hydrothermal process is preferable. Difficulty in controlling the number and species of linked functional group is a major issue for the top-down synthesis technique. The functional groups not only have a profound influence on the electrical band structures of MXenes, and hence on their physical characteristics, but they also have an impact on the surface chemistry and stability of

MXenes. To solve this difficulty, advances in top-down MXene etching techniques and surface functionalization methods are needed. Bottom-up strategies, particularly the CVD process, are predicted to produce MXene with highly regulated chemical compositions and architectures. Other forms of mixed acid etchants, such as HF/H_2SO_4, and their effects on the flake size of each MXene nanosheet can also be mentioned, as MXene flake lateral size is an important aspect of their membrane permeability, selectivity for target pollutants, and fouling potential.[48] Progress in this route of CVD is encouraging, with Mo_2C and MoN obtained. As, this process produces a large area of ultra-thin MXene sheets with a controlled thickness and defect density. However, the CVD method's success is currently confined to Mo-based MXenes with a poor understanding of the growth mechanism. It is envisaged that fundamental understanding gained *via* modeling and experimentation would encourage the synthesis of various MXenes using this cleaner technology. Using this method, giving priority to safety and environmental considerations. In addition, the development process will be directed to investigate alternative non-HF methods. In particular, HF etching was the most frequently used method for delamination of the bulky and rigid MAX phase, without the limitation of a precursor containing "Al" layers.[75,76] Additionally, several experimental factors, including reaction time and etchant concentration, impact the structure and properties of the produced MXene. Few-layered $Ti_3C_2T_x$ and Nb_2CT_x have recently been produced by etching a MAX precursor in one step while adjusting the reaction conditions.[77] But in HF-etched designs, the production of MXene necessitates handling concentrated HF and a time-consuming, multi-step process that produces a toxic and caustic waste liquid.[78] Consequently, techniques utilizing HF etchants *in situ* have been promoted, such as the addition of lithium fluoride (LiF) salt to hydrochloric acid (HCl) or the use of a fluoride etchant such as ammonium bifluoride (NH_4HF_2) salts. However, the use of extremely hazardous etchants and lengthy etching times in standard synthesis methods prevents further investigation of these intriguing 2D MXenes, particularly limiting their biological application. For instance, in hydrolysis or electrochemical processes, the fluoride-residues on the surface of Nb_2CT_x are prone to releasing HF.[79] Fluoride also has an etching effect that degrades equipment, including capacitance. Consequently, there is an urgent need to create safe and efficient fluoride-free synthesis processes.

Chemical etching and other MAX phase exfoliation techniques are often intrinsically electrochemical processes that include electron transport as a component of the surface reaction. As a result, electrochemical etching can be considered as a good substitute strategy to HF etching.[80] Furthermore, the preparation of MXene structures and the resulting properties may be easily controlled by adjusting the voltage, electrolyte, and other operational parameters. The environmental friendliness, durability, and convenience of the electrochemical etching process outweighs other

techniques.[81] However, only a few noteworthy successes have been accomplished, and there are still a lot of challenges and issues with the electrochemical process that need to be resolved. Due to electrochemical polarization, the conditions of the electrochemical etching process for the delamination of bulk MAX precursor are typically different from those used in the conventional electrochemical scenario. This makes it difficult to measure MXene growth and explore the experimental mechanism.[82] Additionally, flash freezing, mechanical milling, or ultrasonication are routinely used to help the delamination process in organic molecules or inorganic salts, which is an effective approach to prepare MXene. Performing delamination under sonication is one approach to resolve the lengthy response time. Micro explosion is a potentially useful strategy that will require more research in the near future. There is a pressing need for more methodical studies on condition optimization for the exfoliation of multilayered MXene. While top-down approaches are the most popular for obtaining MXene, bottom-up approaches are also starting to gain traction.

The bottom-up approach directly creates MXene without requiring derivation from the ternary MAX precursor. The bottom-up approach can achieve more accurate control over designable MXene structures as it builds novel materials atom by atom.[83] This can be useful for producing MXene, which is hard to get using the top-down approach as described above. Thus, several bottom-up techniques have been extensively used to fabricate MXene with regulated shape and thickness.[84,85] To create ultrathin MXene materials, chemical vapor deposition (CVD), is the most widely used technique. Other techniques including template-assisted growth and self-assembly are employed to synthesize MXene with precise structure and form. Previous papers state that MXene may be made on metal layers or graphene using the CVD process, however, there are safety and chemical risks involved due to the conditions needed such as high temperatures or ultrahigh vacuum.[86] There is a need for more sophisticated, inventive, and flexible methods of synthesizing MXene to facilitate future real-world applications.

The current approaches have not yet been widely utilized for full-scale commercialization because of their complexity, high manufacturing costs, and limited efficiency.[87] To address the scalability of MXene production, researchers are exploring high-throughput and automated synthesis methods. Automated chemical etching setups enable the continuous production of MXenes, increasing yield while maintaining high material quality.[20] Novel MXene compositions such as Mo- and V-based MXenes have emerged with enhanced ion selectivity and antimicrobial properties, expanding MXene applications in environmental treatment and desalination.[22] For instance, V_2CT_x and $V_4C_3T_x$ MXenes generated through top-down approaches have shown significant promise for selective ion transport. The development of 3D MXene architectures has introduced innovative solutions to improve water flux and desalination

1016 | *Environ. Sci.: Nano,* 2025, **12**, 1012–1036

This journal is © The Royal Society of Chemistry 2025

performance. By increasing ion transport pathways and mechanical strength, these structures are positioned as promising candidates for future large-scale applications. Additionally, MXene–polymer composites, such as MXene–polyamide (PA) membranes, are emerging as solutions for long-term desalination. These hybrid membranes offer enhanced chlorine resistance, fouling resistance, and durability, making them ideal for water purification.[36]

2.2 Mechanisms and factors influencing desalination

MXene's hydrophilicity and charge characteristics can be altered if the surface termination groups change, significantly influencing the MXene membrane desalination process. However, there are several challenges in managing the surface terminations and size of the artificial MXene-based membranes.[44] Ions intercalated between the interlayers may have an impact on the intrinsic properties of MXenes, such that MXenes generated by the LiF/HCl etching are more suited for use in the creation of membranes. MXene's distinct structure and surface functional groups, such as hydroxyl groups, significantly impacted on how well MXene-based membranes performed.[88] Ma *et al.*[44] utilized a traditional molecular dynamics (MD) simulation to examine the impact of various MXene-based membrane surfaces, such as fluorine (F), oxygen (O), and hydroxyl groups (OH), on the desalination performance of the produced membranes. The simulation demonstrated how both hydrogen bond interactions and surface charge characteristics strongly influence the interactions between the termination group and water. As shown in Fig. 2, the water permeability across MXene channels with various surface terminations follows the order: F > O > OH. The way surface terminations interact with ions is also significantly influenced by their charge state. For example, Na^+ ions are trapped by the negative charge of surface terminations in the MXene membrane channel, such that MXene membranes provide unique Na^+ ion rejection capabilities.[44] In a similar way, the addition of

Ag nanoparticles to $Ti_3C_2T_x$ membranes enhanced the anti-fouling characteristics of the MXene membranes while also considerably increasing the water permeability. To stop the membranes from expanding, Al^{3+} ions can be intercalated into the MXene interlayer due to the strong contacts between the MXene terminating groups and Al^{3+}, resulting in the membranes exhibiting good stability in aqueous solution and having a high rejection of NaCl under fast water flux.[89]

An adequate membrane for desalination needs to have suitable interlayer spacing (which depends on the value of n in the MXene formula $(M_{n+1}X_nT_x)$); the interlayer spacing is frequently in the range of 1 nm, which is effective to repel the bigger hydrated ions, and also maximizes the transit of water molecules through the layers.[90–92] However, MXene exhibits extreme hydrophilicity due to the presence of oxygen, making it highly likely to absorb water and widen the d-spacing between MXene nanosheets in aqueous conditions.[93,94]

To boost the performance and long-term stability of the membranes, it is highly recommended to enhance the mechanical features of MXenes including smoothness and flattening. It has been demonstrated that the swelling effect of hydrophilic laminate membranes has been successfully mitigated by covalent crosslinking.[95] By doing this, it was possible to create inter channels that were densely packed and fixed in place by strong covalent bonds, showing notable improvement over unlinked membranes. High water permeation can still be accomplished, although it is currently challenging to do so without sacrificing separation effectiveness.[96] Thus, the choice of crosslinking procedure, taking the large dimension of the crosslinkers used and their reactive groups into account, is critical for achieving membranes with adequate and fixed 2D capillaries.

Maleic acid is a highly attractive option for linking MXene flakes, with an adequate size of 0.6 nm,[97] and which may operate as reactive binding sites to produce a more efficient MXene with smaller interlayer spacing. MXene's inherent interaction characteristics, hydrophobicity, and slit-shaped
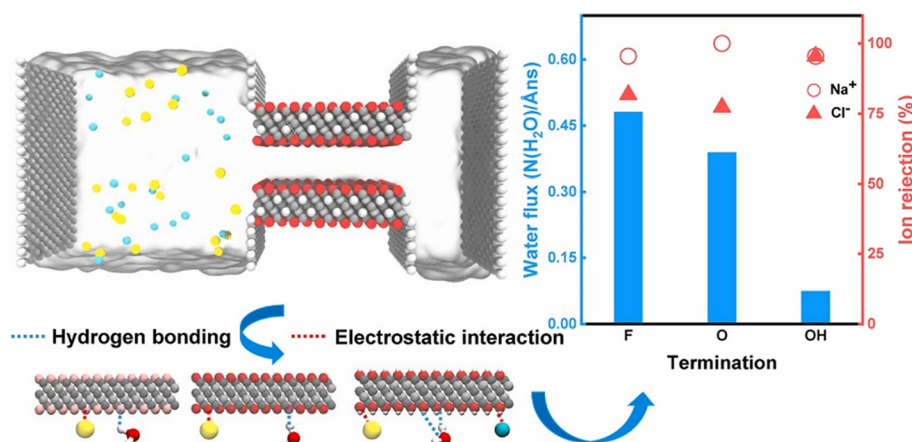

Fig. 2 (Left) Simulation model for the desalination process. (Right) Water flux through nanochannels functionalized with different MXene-based membrane termination groups.[44] Reproduced from ref. 44 with permission from Elsevier, copyright 2022.

This journal is © The Royal Society of Chemistry 2025

Environ. Sci.: Nano, 2025, **12**, 1012–1036 | 1017

pores were discovered to influence the MXene membranes' desalination performance. The utilization of inorganic components promotes water permeability and solvent resistance as challenges to be overcome. Furthermore, at high temperatures (200–500 °C), researchers found that de-functionalization of the MXene film may reduce the interlayer spacing.[98] Hence, for better performance of the MXene membranes, it is necessary to undertake further research exploring the influence of each of the MXene characteristics and the influence of the surrounding conditions on the overall performance of the membranes.

An additional complication is that during the desalination process, salt will crystallize on the surface of the solar absorbers, blocking the channels of water transport and decreasing the energy conversion efficiency, freshwater yield, and stability. Hence, the salt resistance of solar absorbers also becomes a serious issue that needs to be addressed in actual applications. To mitigate this phenomenon, Zhang et al.[99] proposed a Janus structure of the VA-MXA (Fig. 3), thereby realizing the dual functions of solar absorption and water pumping by different layers, in which the hydrophobic upper layer absorbed light and the hydrophilic bottom layer pumped water. As a result, the salts can only precipitate on the hydrophilic layer of the Janus VA-MXA and are then rapidly dissolved due to the continual pumping of water. As a result, the Janus structure significantly reduced salt deposition on the absorbers, allowing the Janus VA-MXA to maintain excellent light absorption on the upper hydrophobic layer for 300 s.[99]

2.3 Performance of MXene-based membranes in water desalination

MXenes have become very attractive nanomaterials due to their unique properties and exhibited exceptional potential in the fabrication of desalination membranes through various methods. The perfect water purification filter and desalination membranes must be antibacterial, ultrathin, with a dense film, robust, and have an important selectivity for small molecules as well as good antibacterial and antifouling properties. For optimum performance, membrane filters have to be antibacterial, thin, physically resilient, have high selectivity, and have excellent fouling resistance.[67,100] As highlighted in Table 1, several approaches have been used to synthesize MXene-based membranes with excellent performance,[101–104] through optimisation of their surface area, exploitation of the convenience of their functionalization, and tailoring of their antifouling capacity,[17,18] mechanical robustness, sieving capabilities, and water transport qualities.[19–21]

For the fabrication of MXene-based lamellar membranes, various methods, including coating-based methods including spray coating, filtration, drop casting and Langmuir–Blodgett have been introduced. MXenes have also been demonstrated to be useful in various applications, mainly those related to the environment, such as membranes, antibacterial agents and capacitive deionization. The high surface area and unique mechanical and electrical characteristics of MXenes make this state-of-the-art material suitable for desalination and water purification.[120–122]

For instance, Ren et al.,[123] reported a freestanding MXene-based membrane using a straightforward vacuum filtration (VF) technique that involved filtering colloidal solutions of delaminated $Ti_3C_2T_x$ to produce membranes characterized by a controllable mass-loading with a thickness of less than 1 nm, and lateral sizes oscillating from hundreds of nanometres to several microns.[123] The occurrence of meso- and macro-pores throughout the membrane is reduced by the high aspect ratio of single-layer $Ti_3C_2T_x$, which guarantees consistent and narrow 2D nanochannels. Such membranes demonstrated exceptional hydrophilic characteristics and remarkable flexibility and mechanical strength, making them ideal for membrane separation.[39] Identified 2D MXene ($Ti_3C_2T_x$) with outstanding properties,
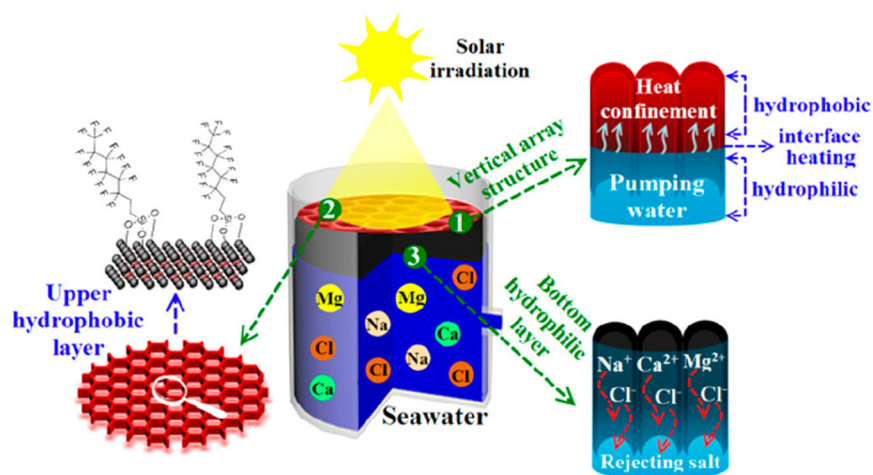

Fig. 3 Vertically aligned MXene-based aerogel with Janus structure of the hydrophobic upper layer and hydrophilic bottom layer designed for solar desalination. Reproduced from ref. 99 with permission from the American Chemical Society, copyright 2019.

Table 1 Summary of state-of-art MXene-based membranes for water desalination

MXene based membrane	Experimental condition (NaCl concentration)	Water presence	Key finding	Ref.
$Ti_3C_2T_x$	10 000 mg L^{-1}	10 L m^{-2} h^{-1} bar^{-1}	• At least 56% less flux drop when compared to an untreated membrane with an MXene coating • Large specific surface area and electrostatic repulsion provide anti-fouling properties	105
$Ti_3C_2T_x$	100–1000 mg L^{-1}	432 L m^{-2} h^{-1} bar^{-1}	• When it comes to separating colours from salts, the composite membrane exhibits effective permselectivity • Because of the lamellar hydrophilic MXene, there is excellent hydrophilicity and flow	106
$Ti_3C_2T_x$	0.2 M	1.1–8.5 L m^{-2} h^{-1} bar^{-1}	• These membranes have a high rejection of NaCl (~89.5–99.6%) • Exhibited good non-swelling stability in aqueous solutions for up to 400 hours	107
$Ti_3C_2T_x$	0.2 mol L^{-1}	10^{-3} mol m^{-2} h^{-1}	• MXene membranes of 575 cm^2 made using potential EPD scale-up method • Excellent ion rejection capability is demonstrated by the EPD-MXene membrane	108
$Ti_3C_2T_x$	0.2 M	0.05–0.06 L m^{-2} h^{-1} bar^{-1}	• An excellent anti-swelling property with high metal ion rejection	109
$Ti_3C_2T_x$–graphene oxide	Co = 10 mg L^{-1}	2.25 L m^{-2} h^{-1} bar^{-1}	• During pressure-driven filtration at 5 bar, the composite membranes efficiently rejected positively charged dye molecules and dye molecules with hydrated radii greater than 5 Å	110
$Ti_3C_2T_x$–graphene oxide	5 mmol L^{-1}	89.6 L m^{-2} h^{-1} bar^{-1}	• High enhanced water permeance, 7.5 times of pristine GO membrane and 2.5 times of GO/TiO_2 membrane	111
$Ti_3C_2T_x$–PSS	0.2 M	0.08 mol m^{-2} h^{-1}	• Highly selective transport of Li^+	112
MXene nanocomposite membrane	Co = 2000 ppm	4.7 L m^{-2} h^{-1} bar^{-1}	• Excellent selectivity and permeability achieved by the produced MXene nanocomposite membrane • Surprisingly consistent performance by MXene nano-composite over 58 day desalination test	113
MXene–CNT	10 mM	23.5 L m^{-2} h^{-1} bar^{-1}	• Numerous short mass transfer nanochannels created the MXene–CNT nanostructure, which enhances water permeance and separation efficiency • MXene–CNT membranes demonstrate controlled swelling by an easy thermal crosslinking procedure	114
PEI/MXene	Co = 50 ppm salt solution	8 L m^{-2} h^{-1} bar^{-1}	• Polyelectrolyte coating improved hydrophilicity & adjusted surface charge • In NF or FO procedure, the membrane demonstrated exceptional water desalination capability	115
PA/MXene	Co = 1000 ppm salts	27.8 ± 2.1 L m^{-2} h^{-1} bar^{-1}	• Finely built NF membranes have a distinctive crumple-structured shape • For the NF membranes, a thinner active layer and a larger filtering area were attained	116
$Ti_3C_2T_x$ MXene–polytetrafluoroethylene (PTFE)	0.36 g L^{-1}	0.77 kg m^{-2} h^{-1}	• 65.3% photothermal efficiency and outstanding temporal responsiveness under intermittent illumination were attained	117
MXene-derived membranes supported on α-Al_2O	—	22.4 L m^{-2} h^{-1} bar^{-1}	• Strong and very thin membranes generated from MXene created, showing good rate of ion rejection. The interlayer spacing of the membranes may be adjusted from 3.71 to 2.65 Å • The decrease in space is attributed to loss of moisture and de-functionalization (–OH) at high temperature inside the MXene film	118
Ag@MXene composite membrane	—	420 L m^{-2} h^{-1} bar^{-1}	• The Ag@MXene composite membrane demonstrated improved bactericidal properties and minimal salt rejection	119

while by combining graphene oxide (GO) and $Ti_3C_2T_x$,[124] created 90 nm thick MXene–GO-based membrane. During pressure-driven filtration at 5 bar, the composite membranes successfully rejected dye molecules with hydrated radii exceeding 5 Å and positively charged dye molecules.

Liu and colleagues created graphene oxide (GO)–MXene-based membranes by the filtering technique.[125] Similarly, Wang et al.[126] produced MXene–CNTs hybrid membranes through vacuum filtration while Liu et al.[127] combined MXene with a polymer matrix to increase the polymer microstructure and physiochemical properties to boost the fabricated membranes' performance. For the reported VF comparative studies, Liu and colleagues also constructed virgin $Ti_3C_2T_x$ incorporating CNTs to improve mechanical

This journal is © The Royal Society of Chemistry 2025

Environ. Sci.: Nano, 2025, **12**, 1012–1036 | **1019**

stability and increase the performance of the prepared membrane.[127] Huang *et al.* used an external field to generate a polyether sulfone (PES)–Ni@MXene membrane and used a wet phase inversion approach to incorporate Ni@MXene into the PES membrane.[128] MXene-based layer-by-layer (LbL) lamellar membranes were also developed,[129] in which LbL assembly was used to assemble a tris(2-aminoethyl) amine (TAEA) and MXene, resulting in a highly ordered MXene/TAEA multilayer,[129] as shown in Fig. 4.

Access to clean water, which is essential for a sustainable society, is becoming increasingly difficult around the world because of population growth, industrial growth, and climate change. Furthermore, emerging pollutants such as heavy metals, microplastics, radionuclides, and pharmaceutical chemicals must be removed to offer and secure safe drinking water.[130] Many investigations have been conducted in this regard to discover novel and creative water-treatment pathways. MXene materials, as detailed in the preceding paragraphs, have physicochemical properties that make them useful for seawater desalination and water purification (pollutants removal).[28] MXenes exceptional qualities, including hydrophilicity, surface/area ratio, low toxicity, and active metallic hydroxide sites, among others, made them easily handled by a variety of processes.[36]

Titanium carbide ($Ti_3C_2T_x$) is the most investigated MXene. Unfortunately, antifouling difficulties plague the commonly utilized water filtration and desalination membranes, lowering membrane life and escalating operational expenses.[131,132] As a result, new materials are being developed with modified membranes' surface characteristics such as hydrophilicity and smoothness as a means to slow down membrane fouling. Additionally, new membrane materials and synthesis techniques create a promising future for the next generation of MXene-based membranes that will significantly improve fouling resistance (Fig. 5).
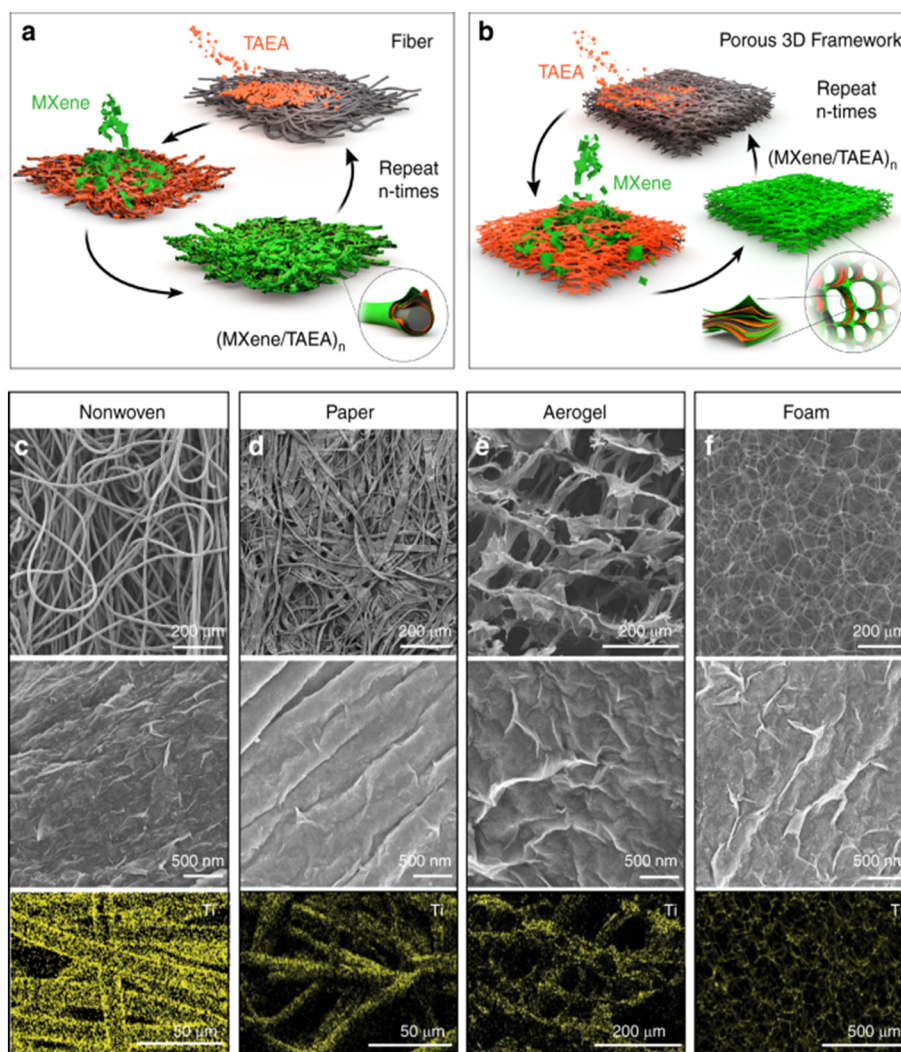

Fig. 4 Layer-by-layer (LbL) assembly of MXene/(tris(2-aminoethyl)amine)$_n$ (TAEA)$_n$ layers on (a) fibres and (b) foams. Physicochemical analysis of MXenes layers coated on different samples of (c) nonwoven, (d) cellulose paper, (e) cellulose nanofibers (CNF) and (f) melamine foam. Reproduced from ref. 129 under a Creative Commons CC BY License.
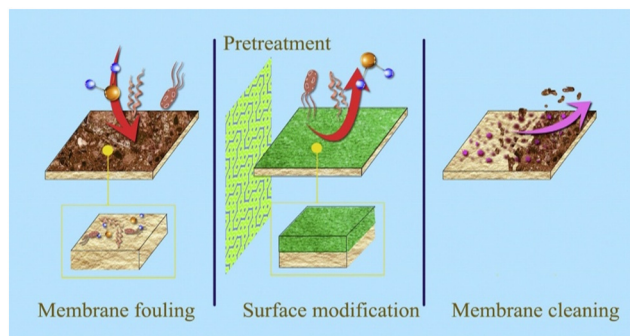
Fig. 5 Membrane fouling occurs due to the deposition of bacterial secretions and the growth of bacteria on surfaces, while surface modification of the membrane can reduce the stickiness or attractiveness of the surface for bacteria, thus reducing the fouling and enabling the membrane to remain clean (unfouled) and functional. Reproduced from ref. 133 with permission from Elsevier, copyright 2017.

Ren *et al.*, exhibited that MXene-based membranes effectively separate Mg^{2+}, Ca^{2+}, Li^+, Al^{3+}, Ni^{2+}, Na^+, and K^+.[123] The permeability of the produced membrane is 37.4 L m^2 h^{-1} bar^{-1}. A 60 nm thick MXene-based membrane for selective separation of NaCl salt was prepared by Pandey *et al.*,[134] which exhibited excellent performance with up to 99.5% separation efficiency. At the same time, water permeance was estimated to be around 85 L m^2 h^{-1} bar^{-1} at 65 °C and the membrane exhibited promising results against biofouling.

A fouling-resistant membrane for seawater desalination with a thickness of 470 nm was developed by incorporating Ag NPs into MXene[94] and exhibited a permeability in the range of 420 L m^2 h^{-1} bar^{-1} using same settings as pure MXene-based membranes. A self-crosslinked MXene-based membrane (SCMM) has been reported,[24] which, when compared to a pristine MXene (16.6 Å), reduced MXene swelling to 15.4 Å and displayed outstanding consistency for 70 hours. SCMMs had a much-reduced penetration rate compared to pure MXene membranes, demonstrating much more effective ion segregation. In a very interesting study, Wang *et al.*,[126] produced a novel membrane with exceptional separation performance, as shown in Fig. 6. Mn^{2+} and Ca^{2+} cations raised the *d*-spacing of a pure MXene membrane from 13.8 to 15.2 Å. These metal cations were used to connect the MXene nanosheets to one another. The *d*-spacing enhanced the selectivity of the MXene-laminates, and the produced membranes demonstrated 100% Na_2SO_4 salt separation while enhancing *d*-spacing.

Han *et al.*,[135] demonstrated dye separation from water using PES/MXene ultrafiltration membranes with water permeance up to 115 L m^2 h^{-1} bar^{-1} and a dye rejection of 92.3%. Another study reported a 90 nm $Ti_3C_2T_x$/GO-based membrane[126] where the interlayer of the $Ti_3C_2T_x$/GO-based membrane was estimated to be 5 Å. A similar $Ti_3C_2T_x$/GO-based membrane was developed by Liu *et al.*,[125] to separate various (textile) dyes from water. The membrane demonstrated an interesting rejection rate (above 99%). The $Ti_3C_2T_x$/GO-based membrane's unusual heterogeneous structure displayed a synergistic impact in substrate rejection and permeability, which changes depending on the relative amounts of GO and MXene. A composite membrane of 550 nm thickness displayed substantially higher water flow (71.9 L m^2 h^{-1} bar^{-1}) than a reference GO membrane (6.5 L m^2 h^{-1}
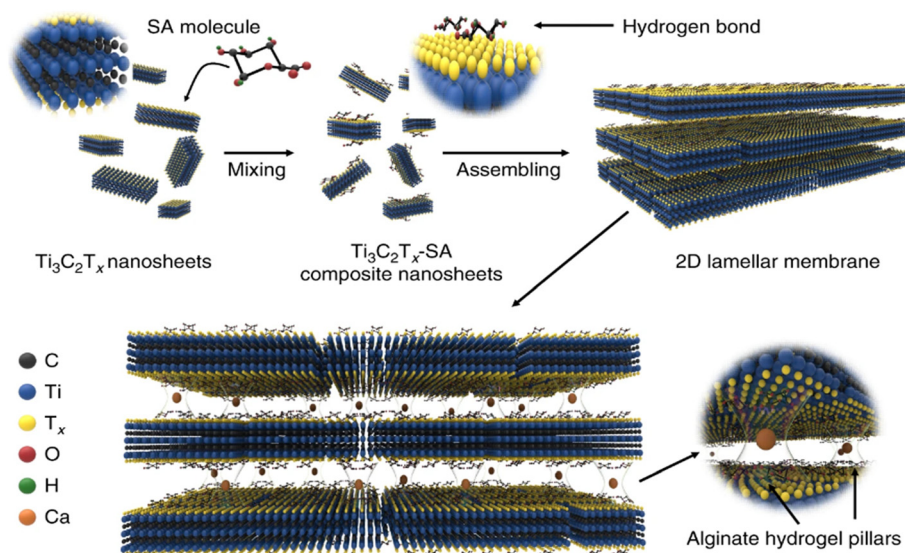

Fig. 6 Synthesis procedure of lamellar $Ti_3C_2T_x$ membranes. The SA molecules were strongly and uniformly bound to the nanosheet surface through hydrogen bonding. The composite SA–$Ti_3C_2T_x$ nanosheets were then linked together to form a hybrid SA–$Ti_3C_2T_x$ membrane with a lamellar structure. As a final point, the SA–$Ti_3C_2T_x$ membrane was submerged in multivalent Mn^+ cross-linking solution to create the cross-linked membrane with interlayer spacing hydrogel pillars. Reproduced from ref. 126 which is published under a Creative Commons CC BY License.

bar^{-1}) under the same testing circumstances owing to its favourable two-dimensional (2D) interlayer channels and hydrophilicity. The study demonstrated that several parameters, such as temperature, pressure, and water absorption, may influence the microstructure and the performance of the MXene membrane. Ding and colleagues[45] used a VF process to produce a unique 2D MXene membrane with a very short transport pathway and enormous nanochannels amounts that display excellent water permeance (more than 1000 L m^2 h^{-1} bar^{-1}) and a reasonable rejection rate (over 90%) for molecules with sizes of approximatively 2.5 nm. This water permeance is superior to the extensively studied membranes with comparable rejections. $Ti_3C_2T_x$ membrane with embedded colloidal $Fe(OH)_3$ was evaluated in terms of the capability of the prepared membranes to separate molecules with sizes larger than 2.5 nm (Fig. 7). More than 90% of molecules with sizes larger than 2.5 nm were rejected by the membrane.[45]

Mahar et al.,[136] developed an excellent membrane with a water permeability of 268 L m^2 h^{-1} bar^{-1} and 99% dye rejection. MXene/polysulfone (PSF) ($Ti_3C_2T_x$) membranes with 99% bovine serum albumin (BSA) rejection and good permeability up to 218 m^2 h^{-1} bar^{-1} were reported by Shen et al.[137] Wang and colleagues created a $Ti_3C_2T_x$/CNTs hybrid membrane for precious metal recovery, specifically gold (Au).[138] In comparison with the pure MXene membrane, the as-prepared MXene–CNT membranes exhibited 200% better performance, collected up to 99.8% Au, and had a water permeance of 437.6 L m^2 h^{-1} bar^{-1}.

Due to its hydrophilic nature, MXene, like GO laminates, has a high water permeance. Moreover, ions having a higher charge (>2) and hydration radii less significant than the interlayer gap of MXene (i.e., <6 nm) permeated more slowly than singly charged cations. However, MXene, comparable to other 2D materials, swells in water and delaminates rapidly due to electrostatic and hydrogen bonding, which reduces membrane separation effectiveness. Meng et al.,[52] suggested a novel desalination membrane

based on surface-charged laminar-stacked MXene (SC-MXene) that was simply manufactured by MXenes stacking and coated with a polyelectrolyte layer (Fig. 8a and b). During either the nanofiltration or forward osmosis processes, the prepared membrane demonstrated very interesting separation performance and avoided the main problem of MXene, which is related to its weak(mechanical) bonding to the substrate, such that the fabricated membranes remained stable and were difficult to delaminate and destroy. The SC-MXene membrane showed excellent separation performance, signifying the promising potential in the future for water desalination.

Liu and colleagues discussed constructing and testing a new composite membrane based on MXene and GO.[66] Under optimized conditions, the synergic effect of GO and MXene significantly improved the performance of the membranes, mainly in substrate rejection, water permeability and stability of the membranes. Because of its superior interlayer channels, the MXene/GO-based membrane demonstrated higher permeance (71.9 L m^2 h^{-1} bar^{-1}), while the operational stability of this membrane was about one month.

Ensuring precise regulation of water transport in nanochannels and nanopores is crucial for water treatment purposes. There is a growing interest in creating intelligent membranes that can react to various stimuli such as temperature, pH, light, pressure, ions, magnetic fields, and electric fields. Among these stimuli, electric fields are especially appealing due to their ability to offer accurate and fine-tuned control.

Zhang et al.[139] conducted a study on $Ti_3C_2T_x$ MXene membranes and observed a remarkable 70-fold increase in water permeation when a negative voltage was applied. Using density functional theory, they investigated the atomic-level interactions between MXene and water under the influence of an electric field. The experimental findings indicated that the negative voltage facilitated a stronger water/MXene interaction, resulting in an accelerated water permeation rate as water molecules more effectively entered the MXene film's interlayer. This research underscores the significant impact of electric fields on water transport within MXene membranes. Moreover, optimizing the surface chemistry of MXene sheets could further enhance this interaction, opening up possibilities for advanced smart membrane technologies. Meng et al.[140] fabricated a surface-charged membrane by wet-etching Ti_3AlC_2 powders to form ultra-thin $Ti_3C_2T_x$ MXene nanosheets, which were assembled into a laminar structure for desalination. Adjusting the MXene nanosheet loading allowed them to control the membrane's thickness. By coating the membrane with polyethyleneimine, they manipulated its surface charge. Compared to other 2D material membranes (graphene oxide and MoS_2 membranes), the $Ti_3C_2T_x$–polyethyleneimine MXene membrane exhibited significantly superior desalination performance whereby in forward osmosis, its water/salt selectivity was one order of magnitude higher. In nanofiltration, it demonstrated higher salt rejection rates. These exceptional results were achieved
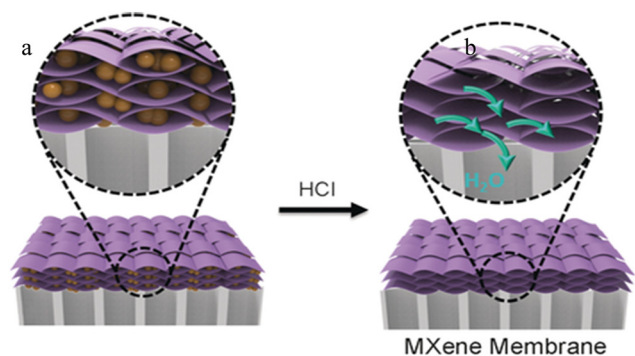

Fig. 7 (a) 2D MXene nanosheets based membrane with colloidal $Fe(OH)_3$ (yellow spheres). (b) Hydrochloric acid solution (HCl) treatment to remove the $Fe(OH)_3$ nanoparticles from the synthesized MXene. Reproduced from ref. 45 with permission from Wiley, copyright 2017.
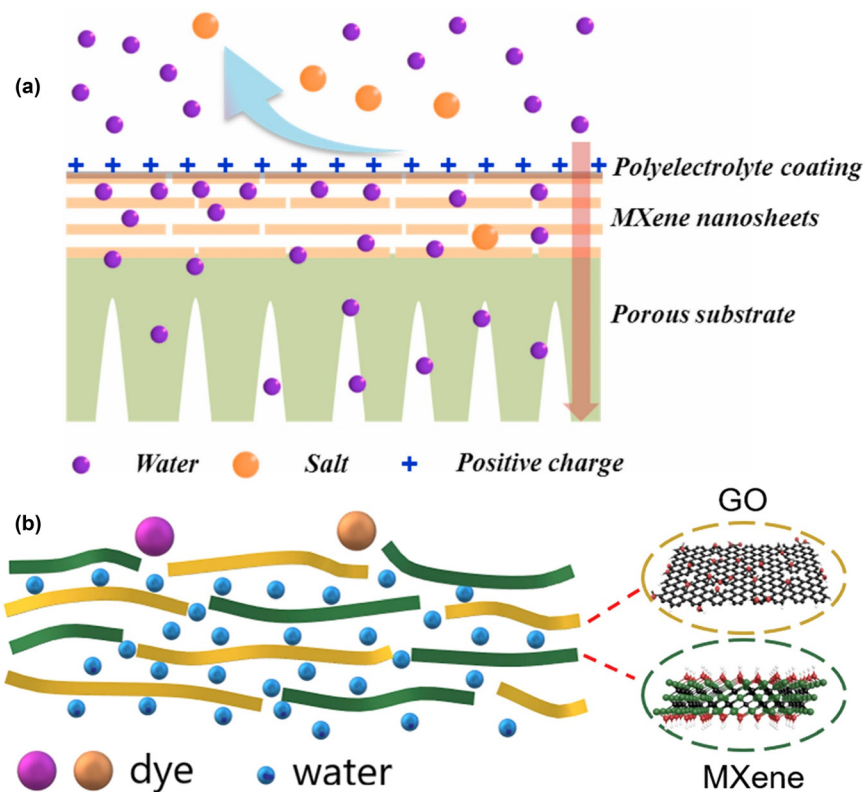
Fig. 8 (a) Laminar stacking of MXene nanosheet based membrane with a polyelectrolyte surface coating (SC). Reproduced from ref. 52 with permission from Elsevier, copyright 2021. (b) GO/MXene composite membranes were fabricated for water treatment. Reproduced from ref. 125 with permission from Elsevier, copyright 2020.

through size sieving and electrostatic repulsion mechanisms.[140] The polyethyleneimine coating improved hydrophilicity and prevented excessive swelling, maintaining effective interlayer size sieving. However, the PEI coating introduced some transport resistance, leading to a permeability–selectivity trade-off.[140] Nevertheless, surface-charged MXene PEI membrane remains a promising candidate for water desalination and selective ion transport applications. The optimal PEI concentration can be chosen for the PEI layer, as water permeability decreases due to the increased transport resistance associated with the PEI coating. Future optimization of the PEI coating may help address this trade-off and further enhance the membrane's overall performance. Wang *et al.*[141] developed innovative hybrid carbon nanofibers using MXene as a base material, encapsulated with electrochemically polymerized polyacrylamide. These nanofibers served as efficient asymmetrical electrodes in membrane capacitive deionization (MCDI) for wastewater desalination. The continuously high conductivity of the hybrid nanofibers led to an abundance of adsorption sites and shortened charge carrier paths, significantly increasing the specific capacitance, salt removal capacity of these hybrid nanofibers relative to the unfunctionalized carbon nanofibres. As a result, the MCDI electrodes demonstrated an impressive desalination capacity of 92 mg g^{-1} and selectively adsorbed divalent ions from

high-salt water containing multiple charged species.[141] This advance makes MCDI technology a competitive and effective solution for desalinating saline wastewater.

The use of MXene-based membranes with electrochemically active polyacrylamide represents another promising step forward in membrane capacitive deionization for water desalination applications. Chen *et al.*[142] developed an MXene-based membrane for desalination. Interestingly, when subjected to an alternating current electric field during desalination, this membrane exhibited a peculiar inductive effect in ion diffusion. The authors observed that the strength of this inductance was reduced with higher electrolyte concentrations and longer immersion times.[142] The ion confinement by the MXene sheets within the membrane caused this inductive action. To analyze the experimental data, the team employed a backpropagation neural network, revealing that the type and concentration of the electrolyte had a more significant influence on the inductive effect compared to the immersion time.[142] These findings indicate that the inductive signals of the membrane can be controlled and adjusted by utilizing 2D materials such as MXene. This exciting discovery holds promise for designing membranes with customizable inductive properties for various applications. Li *et al.*[143] conducted a study to explore how the separation performance of conductive Ti$_3$C$_2$-T$_x$ lamellar membranes for dye molecules can be

This journal is © The Royal Society of Chemistry 2025

Environ. Sci.: Nano, 2025, **12**, 1012–1036 | **1023**

manipulated by an external electric field. They found that the membranes' separation abilities vary depending on the charge characteristics of the dyes: when faced with cationic dyes, applying a negative voltage enhanced the membranes' sieving efficiency but decreased the water flow; conversely, a positive electric field decreased retention capacities while simultaneously improving water flux for cationic dye solutions.[143] However, the electrified $Ti_3C_2T_x$ nanofiltration membranes displayed entirely distinct patterns when dealing with anionic dye solutions, regardless of the voltage's polarity. The impact of an external electric field on the separation efficiency of $Ti_3C_2T_x$ membranes arises from alterations in electrostatic interaction. This research demonstrates the possibility of controlling the sieving capabilities of MXene membranes through the application of an external electric field. Feng et al.[144] used a one-dimensional model enhanced to include an external electric field to replicate the flux of cation penetration and rejection in an MXene membrane. They validated the model's accuracy by comparing its predictions with experimental data. Through optimization of parameters in both operational modes, the researchers effectively simulated the permeation and rejection of ions through the membrane.[144] Both the experimental and simulated results consistently pointed out the significant role played by interlayer spacing in influencing membrane performance. This underscores the critical importance of interlayer spacing in controlling ion transport. By using and adapting this theoretical model, valuable insights were gained that can guide future membrane design and help assess a membrane's suitability for applications in water desalination computationally before it is developed, as part of the safe by design approach.[145,146]

Fan et al.[147] introduced a 2D MXene membrane that can efficiently separate K^+ and Pb^{2+} ions under an external voltage. The MXene membrane exhibited an impressive rejection rate of up to 99% for hydrated Pb^{2+} ions, while allowing smooth transport of hydrated K^+ ions through its channels. Even with a thickness of 365 nm, the separator factor for a mixture of K^+ and Pb^{2+} ions reached a remarkable 78 at an application of 17 V. Additionally, the MXene membrane remained stable without swelling when subjected to an external voltage, ensuring effective rejection of Pb^{2+} ions.[147] The remarkable ability of the membrane to effectively reject Pb^{2+} ions and its resistance to swelling highlight its stability. This study provides compelling evidence for the considerable promise of MXene membranes as a viable option for ion sieving and the selective removal of ions. The inherent stability and anti-swelling characteristics of these two-dimensional MXene ($Ti_2C_3T_x$) membranes make them highly suitable for applications in ion sieving and water purification, particularly when subjected to an external voltage. Ren et al.[148] developed a specialized nano-channeled $Ti_3C_2T_x$ MXene membrane capable of regulating the passage or retention of both inorganic ions and organic dye molecules through the application of an electrical potential. By using a negative electrical potential, the membrane's ability to reject inorganic salts was enhanced. Conversely, applying a positive
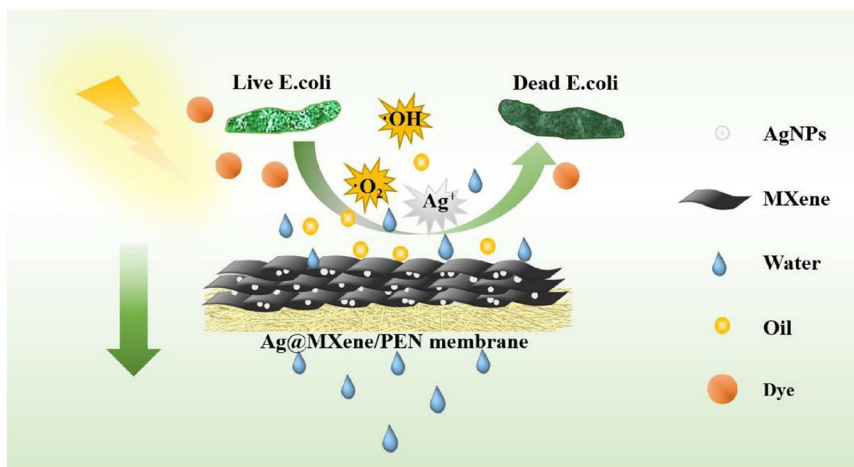
potential hindered rejection.[111] In their experiments using a flow-through system, the researchers assessed the rejection rates of membranes. Even ultra-thin membranes, with a thickness of only 100 nm, demonstrated an impressive rejection rate exceeding 98% for methylene blue dye molecules. This voltage-controlled rejection, made possible by electronically conductive membranes, holds considerable promise as an effective approach to enhance the filtration of inorganic and organic compounds. Wang et al.[149] presented an innovative MXene membrane that maintains a consistent interlayer spacing of around 1 nm and shows remarkable ionic conductivity at critical solution concentrations. By applying different gate voltages to the membrane, they successfully showcased the capability to reversibly control ion conductivity. Surprisingly, the ion conductivity increased almost ten times more under a positive voltage than it did under a negative one because the negative potential accumulation resulting from the negative voltage inhibits ion transport, attracting an increasing number of positive balancing ions into the MXene membrane.[149]

Based on the analysis presented above, the physicochemical characteristics and performance of MXene membranes could be improved by regulating the pore structure through appropriate intercalation or crosslinking. In addition, to further boost the permeance and improve the selectivity of MXene membranes, future research and demonstration efforts should focus on understanding the intercalations and how they impact the performance of the membranes. On the other hand, even though MXene membranes show exciting separation properties, there remains a technical challenge to scale up production to a large enough membrane area with tolerated amounts of defects for practical application. The deficiency of low-cost, chemically stable commercial membranes demonstrated a main obstacle in the early development and commercialization of MXenes-based membranes. The ideal MXene-based membrane for water treatment and/or desalination must have favourable chemical stability toward the physicochemical changes during the separation process, low permeability, and high proton conductivity. It must be capable of withstanding fouling from impurities so the membrane will remain efficient and sustainable.
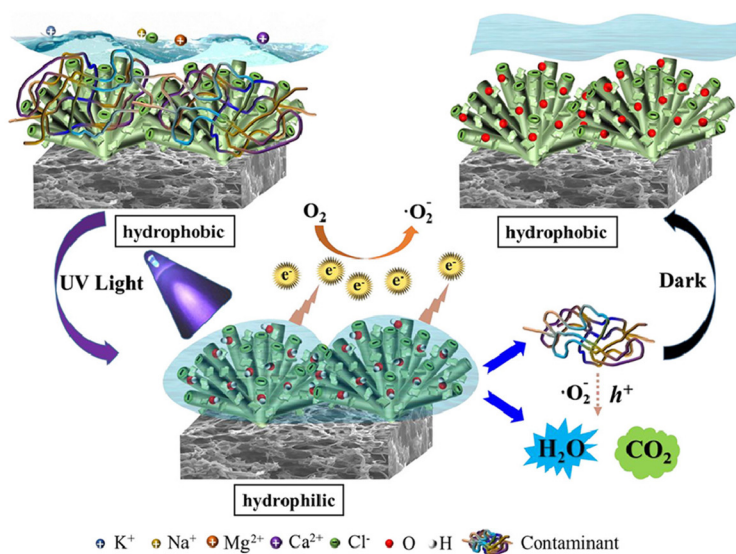
3. MXene-based membranes and their antibacterial activity

Viral or biological contamination, which causes many waterborne ailments, is regarded as potentially the most harmful global problem,[150,151] and is a key aspect of membrane fouling. Because biofouling affects the performance of the membranes, the antibacterial qualities of membranes must be studied. Recently, several materials, including MXenes, carbon-based materials, metals and metal oxide nanoparticles (NPs) have been explored as bactericidal nanomaterials, investigating their antibacterial activity against Gram-negative and Gram-positive microbes[152–156] (Fig. 9a and b).

Fig. 9 (a) Antibacterial activity of MXene. The laminar nature of the MXene causes them to intertwine with bacteria resulting in membrane damage and death. Reproduced from ref. 155 with permission from Elsevier, copyright 2022. (b) Antibacterial and fouling-resistant covalently cross-linked MXene-based membrane. Reproduced from ref. 156 with permission from Elsevier, copyright 2022.

MXenes, with their distinct hydrophilic characteristics, great adsorption and optimal surface functioning, have already opened new doors for water desalination and water treatment. Moreover, MXenes are believed to be antimicrobial and thus biofouling resistant (Fig. 10) and may offer promising antibacterial performance.[134,155,157] The membranes outperformed GO membranes in terms of antibacterial activity against Gram-negative *Escherichia coli* (*E. coli*) and Gram-positive *Bacillus subtilis* (*B. subtilis*). Fig. 10 shows the antibacterial activity of MXene-based membranes against *B. subtilis* and *E. coli* after filtering a bacterial solution containing[152] colony-forming units (CFU) per mL compared to the polyvinylidene difluoride (PVDF) membrane control. After 24 hours of incubation with $Ti_3C_2T_x$ modified PVDF membranes, a decline in the number of viable colonies of *B. subtilis* and *E. coli* was observed (Fig. 10A).

As a result, MXene layers were able to minimize bacterial culture and diminish bacterial cell life when compared to pristine PVDF membranes. $Ti_3C_2T_x$ membranes limited *B. subtilis* growth by 73% and *E. coli* growth by 67% compared to control PVDF membranes (Fig. 10B). Compared to the control PVDF membranes, the composite PVDF–MXene membranes had a bactericidal rate between 63% and 73%.[158] Moreover, the $Ti_3C_2T_x$ membrane reduced the growth of both bacteria by more than 99% under similar conditions. Mayerberger *et al.* proved that electrospun $Ti_3C_2T_z$/chitosan composite nanofiber membranes have very promising antibacterial performance, demonstrating a 95% and 62% decrease in colony forming units, respectively, after four hours of treatment with the 0.75 wt% $Ti_3C_2T_z$ – loaded nanofibers.[159]

This journal is © The Royal Society of Chemistry 2025

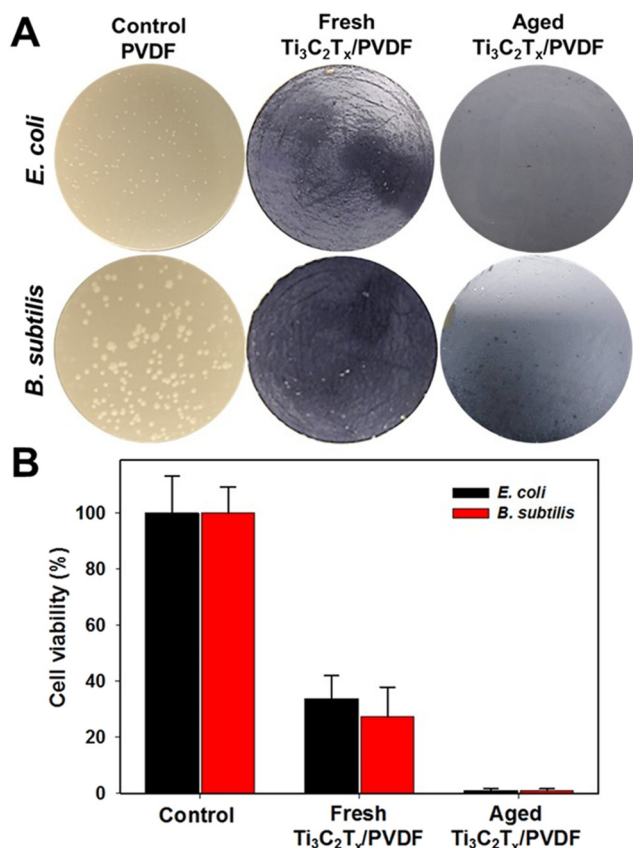*Environ. Sci.: Nano*, 2025, **12**, 1012–1036 | **1025**

Fig. 10 (A) Antibacterial activity of $Ti_3C_2T_x$ MXene membrane. (B) 24 cell viability measurements of *B. subtilis* and *E. coli* after exposure to the $Ti_3C_2T_x$ MXene membrane for 24 hours. Reproduced from ref. 158 which is published under a Creative Commons Attribution 4.0 International License.

Another study demonstrated how the antimicrobial effect and overall toxicity of MXene were modified by the addition of various ceramic oxide and noble metal NPs; Gram-negative *E. coli* colony-forming units were decreased by 95% and Gram-positive *Staphylococcus aureus* (*S. aureus*) colony-forming units were reduced by 62% in the as-prepared composite membrane. Green algae (*Desmodesmus quadricauda*) and two higher plants, sorghum (*Sorghum saccharatum*) and charlock (*Sinapis alba*), were tested for ecotoxicity. The findings demonstrated that the NP–MXene composites obtained could have both stimulating and inhibitory effects on algae, and the ecotoxicity was dependent on the dose and kind of modification.[160]

The antibacterial characteristics of $Ti_3C_2/SiO_2/Ag$, $Ti_3C_2/Al_2O_3/Ag$, and $Ti_3C_2/SiO_2/Pd$ nanocomposite membranes were investigated by Jastrzębska *et al.*,[161] who also demonstrated that Ti_2C and Ti_3C_2 MXenes were extremely bioactive against a Gram-negative bacteria strain of *E. coli*. Utilizing near-infrared (NIR) light, Zhu *et al.*,[162] studied the antibacterial activity of silver (Ag), $Ti_3C_2T_x$, and an $Ag/Ti_3C_2T_x$ composite membrane. The as-prepared $Ag/Ti_3C_2T_x$ composite indicated the best antibacterial efficacy against the studied bacteria of the composites tested. NIR irradiation significantly improved the antibacterial activity of $Ag/Ti_3C_2T_x$ compared to virgin Ag and $Ti_3C_2T_x$. For the first 0–6 h, 200 g mL^{-1} $Ti_3C_2T_x$ completely repressed *E. coli* expansion owing to the photothermal heat generated, which killed the bacteria in the surrounding region. The $Ti_3C_2T_x$ composite could completely prevent *E. coli* growth when administered at 100–200 g mL^{-1} after NIR irradiation.[162]

4. Interfacial solar steam generation using MXene

By using a solar evaporator to capture sunlight and concentrate heat at the air–water interface, the interfacial solar steam generation (ISSG) approach helps to enhance water evaporation. Effectively absorbing a wide range of solar radiation, converting it to heat, and concentrating that heat at the evaporation location are the requirements for the solar evaporator. It should also be able to move water to areas where heat is concentrated by absorbing different amounts of water. Different kinds of photothermal materials are used to form the evaporator's solar-absorbing surface. Depending on the light to heat conversion mechanism, the photothermal materials are generally categorised as (i) carbon-based materials (conjugation/hyperconjugation effect of electrons), (ii) semiconductor-based materials (generation and relaxation of electron and hole pairs) and (iii) plasmonic materials (localize surface plasmon resonance).[163] The photothermal conversion mechanism of MXene is not yet fully realised however, most researcher consider that the photothermal conversion occurs in MXene due to localize surface plasmon resonance (LSPR).[164,165] LSPR occurs in the presence of light, when the natural metal surface electron frequency matches the frequency of the incident photons.[163] When these photons are absorbed by a metal surface, the excited electrons rise above the Fermi level, causing oscillations in the electron gas. This process results in the creation of hot electrons. The plasmonic material's surface temperature rises quickly when hot electrons decay *via* electron–electron scattering rather than radiative emission, causing the hot electrons' energy to be redistributed. Ti_3C_2 is the most often utilized MXene material in the field of ISSG. Li *et al.* produced an MXene membrane utilizing a vacuum filtration approach, demonstrating for the first time the utilization of Ti_3C_2 in this sector with an outstanding light to water evaporation efficiency of 84% under 1 sun.[166] Moreover, they used a droplet laser heating process (wavelength of 473 nm and 785 nm) to show that MXene (Ti_3C_2) has excellent internal light to heat conversion efficiency of 100%. From the UV-vis-NIR spectra of Ti_3C_2 nanosheets, Lin *et al.* observed a unique absorption in NIR region (750–850 nm) similar to the plasmonic material like Ag and Au.[167] Fan *et al.* observed two enhanced absorption peaks at 610 nm and 1148 nm in their composite ($PEG/Ti_3C_2T_x$) and attribute it to the LSPR effect of $Ti_3C_2T_x$ nanosheets.[168] Chaudhuri also claimed that arrays of $Ti_3C_2T_x$ nano disk shows strong LSPR effect in near infrared frequencies.[169] Moreover, Shahzad *et al.* observed that MXene

1026 | *Environ. Sci.: Nano*, 2025, **12**, 1012–1036

This journal is © The Royal Society of Chemistry 2025

($Ti_3C_2T_x$) has Electromagnetic Interference (EMI) shielding property due to its outstanding electrical conductivity (4600 siemens per cm) and capability of absorbing electromagnetic waves (EMW) by multiple internal refection inside $Ti_3C_2T_x$ layers.[170] This property of absorbing EMW makes MXene an excellent photothermal material for ISSG application. Absorbing broad spectrum of sunlight effectively is one of the most important tasks of an efficient solar evaporator. To enhance light absorption by light scattering and multiple internal reflection, Li *et al.* prepared a biomimetic 2D material nanocoating composed of MXene ($Ti_3C_2T_x$), reduced graphene oxide (rGO) and MoS_2 that demonstrated broadband light absorption up to 93.2%.[171] Similarly, Cai *et al.* prepared MXene@MoS_2 nanoflower for increasing the light absorption as well as photothermal conversion capability of the solar absorber utilizing the internal reflection of light and the synergistic effect of MXene and MoS_2.[172] Except these many article demonstrates the use of MXene as photothermal material for solar steam generation application.[173–175]

Another advantage of using MXene in ISSG application is its inherent hydrophilicity due to the presence of surface functional groups (*i.e.*, –OH, –O, –F).[143,145,168] Therefore, the solar absorbing surface containing MXene can absorb water faster and facilitate water evaporation at air water interface. More water may evaporate from a hydrophilic solar-absorbing surface than from a hydrophobic one.[176] However, hydrophobic solar absorbing surface are better for salt rejection. The solar absorbing layer composed of MXene based photothermal material can be made hydrophobic and are generally found in Janus solar evaporator where water evaporation occurs at hydrophobic–hydrophilic interface. In such evaporators the hydrophobic solar absorbing layers are kept thin to make the vapor escape route shorter.[177] Long term stability of the solar evaporator in a complex water system (*i.e.*, seawater or wastewater *etc.*) where many microbials are present is another important factor for ISSG based water purification/desalination system. It has been demonstrated that MXene coating is an extremely effective bacteriostatic agent that may harm bacterial membranes and prevent Gram-positive and Gram-negative bacteria from growing on solar evaporator surfaces.[178] Therefore, it can be stated that MXene is a very desirable photothermal material in the field of ISSG due to its high light absorbing capability, photothermal conversion capability, inherent hydrophilicity and resistance against bacterial growth.

4.1 Salt-rejection properties of MXene based evaporator

One of the main obstacles to applying the ISSG-based water desalination system in the real world is the development of salt crystals on the evaporator's solar-absorbing surface. The salt crystal reduces the water evaporation capability of an evaporator by reflecting sunlight and blocking the water transport channel. Moreover, excessive growth of salt may cause cracking of the internal microchannel of the evaporator and thus reducing the lifetime. There are many ways to solve this issue. However, in MXene-based solar evaporators, the following approaches are mostly observed to stop the salt crystallization on the top of solar absorbing surface: (i) salt ion diffusion back flow (ii) edge preferential salt crystallization and (iii) salt blocking by Janus structure. During seawater evaporation, the evaporator absorbs tuned amount of water and transport it to the solar absorbing surface where heat is localised. The salt concentration of water layer at air–water interface gradually increases due to rapid vaporization of water. Salt crystallization occurs if sufficient water is not transported to the top solar absorbing surface. By delivering enough water to the sun absorbing surface through its internal microchannels, the salt ion diffusion reverse flow process extracts salt from the top solar absorbing surface and returns it to the bulk sea water. As a result, the porosity and hydrophilicity of the solar evaporator, which are greatly impacted by substrate preparation, intrinsic porosity, and coating method, are key components of this process. Saleque *et al.* utilised MXene/MnO_2 coated luffa sponge to desalinate seawater.[175] The inherent porous structure, micro channel networks of the luffa sponge and the hydrophilicity of the evaporator supplied adequate amount of water to the top surface of the evaporator, which kept it moist and facilitated salt diffusion and transferred the salt ions back to the bulk water. Bai *et al.* utilised chemical treatment method to remove hydrophobic lignin from raw coconut husk, which enlarged the internal pores and increased the hydrophilicity of the substrate. This modification enhanced water transportation that facilitated the transfer of salt ion back to the bulk water.[179] Fan *et al.* demonstrated the effectiveness of MXene/PPy modified asymmetry sponge in solar desalination, where melamine foam was used as a substrate for its inherent open network and high porosity (96.8%) to facilitate salt ion diffusion backflow (as shown in Fig. 11a).[180] Sun *et al.* prepared a MXene based aerogel using directional freeze drying process for ISSG application and compared it with an aerogel prepared by non-directional freeze drying process to demonstrate that the channel formed due to directional freeze drying facilitates salt diffusion mechanism.[181] A salt ion diffusion backflow mechanism has been included into prepared evaporators by several researchers in an effort to prevent the formation of salt crystals on the evaporator's surface.[182,183] The effectiveness of edge preferential salt crystallization (sometimes known as localised salt crystallization) mechanism mainly depend on the water transport route.[163] This mechanism is normally observed in evaporators with 1D water transport route. Water travels along a 1D path to reach the center of the solar-absorbing surface in such an evaporator. The solar absorbing surface gets wet from the center outward in a radial orientation, which causes the water evaporating at the evaporator's border to have a greater salt content than the evaporator's center. As a result, the salt begins to form along the evaporator's edge, preventing salt crystals from growing throughout the majority of the solar-absorbing surface. With time the amount of
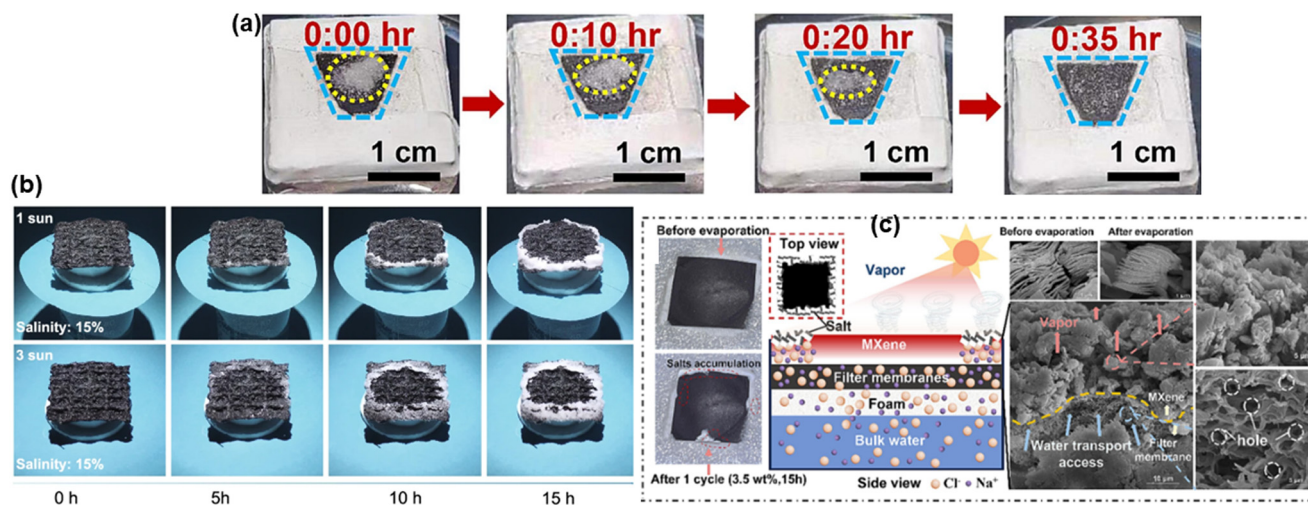
This journal is © The Royal Society of Chemistry 2025

Environ. Sci.: Nano, 2025, **12**, 1012–1036 | **1027**

Fig. 11 Salt rejection: (a) salt dissolved in the solar absorber over time with one sun irradiation.[180] Reproduced from ref. 180 with permission from Elsevier, copyright 2024; (b) salt growth under the irradiation of 1 and 3 solar intensities with salt concentration of 15%.[184] Reproduced from ref. 184 which is published under a Creative Commons Attribution 4.0 International License. (c) No salt growth in the centre of the evaporator due to hydrophobic characteristic of the surface.[186] Reproduced from ref. 186 with permission from Elsevier, copyright 2023.

accumulated salt increases at the edge and falls from it due to gravitational force. Lei *et al.* utilised a 1D water transport route with their MXene decorated 3D honeycomb fabric-based evaporator to introduce edge preferential salt crystallization mechanism and produce water and salt simultaneously (as shown in Fig. 11b).[184] Li *et al.*, prepared a PVA hydrogel-based 3D evaporator where MXene was used as photothermal materials.[185] In order to promote edge-preferential salt crystallization, they have customized a conical frustum 3D structure to guarantee water spreading from the center to the radial direction. Another frequently used method for preventing salt accumulation on the surface of MXene-based evaporators is salt blocking *via* the Janus structure. These evaporators feature two sorts of surfaces: hydrophilic for absorbing water and hydrophobic for absorbing solar radiation. While the hydrophobic sun absorbing surface prevents water from rising to the top and causes evaporation to occur at the hydrophobic–hydrophilic boundary, the hydrophilic surface absorbs water and transfers it to the top.

During solar evaporation, the salt concentration of water at the interface increases but the hydrophilic surface pumps enough water to keep the salt dissolved at the interface and transfer it back to the bulk water. Without any evidence of salt crystallization at the sun absorbing surface, the Janus evaporator can run for an extended period of time. But since water evaporates at the hydrophobic–hydrophilic boundary, it is advised to keep the hydrophobic surface thin in order to increase the rate of evaporation by reducing the length of the heat conduction channel and vapor escape route.[176,177] By creating an aerogel based on Janus MXene and adjusting the amount of a solution containing fluorinated alkyl silane, Zhang *et al.* demonstrated that the rate of water evaporation rises as the hydrophobic layer's thickness decreases.[177] As MXene is inherently hydrophilic, chemical treatment or other hydrophobic materials/substances are required to be utilised with MXene to prepare the hydrophobic solar absorbing surface of the Janus evaporator.

Li *et al.*, fabricated a Janus evaporator by spray coating hydrophilic PLA (polylactic acid)/TiO₂ nanofluid membrane with hydrophobic solar absorbing solution prepared by mixing MXene with polydimethylsiloxane (PDMS).[187] Li *et al.*, prepared a MXene-based Janus membrane for solar steam generation where perfluorodecyltrimethoxysilane (PFDTMS) was used as hydrophobic agent. The prepared solar evaporator demonstrated photothermal evaporation rate and solar thermal conversion efficiency of 1.53 kg m^{-2} h^{-1} and 85.6% respectively with 93% light absorption capability.[136] Su *et al.* demonstrate that due to the hydrophobic nature of the surface the salt does not grow at the centre of the evaporator as shown in the Fig. 11c.[186]

4.2 Fluid transfer performance

Wu *et al.*,[188] presented an innovative anisotropic Ti₃C₂T$_x$/carbon nanotube-based aerogel featuring vertically aligned channels and high porosity, achieved through a directional freeze-drying process. The schematic illustrating the mechanism of water evaporation within the aerogel is depicted in Fig. 12a. Notably, the dimension of vertical channels can be modified by varying the mass ratio of Ti₃C₂-T$_x$ to CNT. The anisotropic Ti₃C₂T$_x$/CNT aerogel, characterized by an average vertical channel size of 80 μm (as shown in the SEM image in Fig. 12b), demonstrated a remarkable capillary effect that significantly enhanced water transport. This design resulted in a high light absorption rate and energy efficiency of 94%. Consequently, the aerogel achieved impressive water evaporation rates of 2.1 and 2.0 kg m^{-2} h^{-1} using water and seawater under 1-sun illumination, underscoring the critical role of the capillary effect in

facilitating water transport. Zhang et al.,[189] developed three-dimensional MXene–sodium alginate aerogel evaporators, maintaining a constant MXene content to improve solar steam generation and long-term desalination efficiency. They systematically examined the performance of these aerogels by varying the sodium alginate content, adjusting its mass ratios from 10 to 40 wt% within the MXene–sodium alginate composite. The resulting composite aerogels featured a distinctive structure formed through the interaction of sodium alginate chains with MXene nanosheets via hydrogen-bonding networks and ionic cross-linking. By modulating the sodium alginate ratio, the pore structures of the aerogel could be effectively optimized, enabling rapid water transport from the bulk to the evaporation interface. A schematic illustrating the states of water surrounding sodium alginate in the aerogel is provided in Fig. 12c. The aerogel demonstrated remarkable evaporation performance, owing to its optimal pore structures, effective water activation, and exceptional photothermal conversion capacity. Additionally, the produced aerogel exhibited a notably low density of approximately 24 mg cm^{-3}. The scanning electron microscopy images in Fig. 12d reveal a honeycomb pore structure that is advantageous for water transfer during the desalination process. Importantly, the aerogel with 30 wt% sodium alginate showcased outstanding desalination capabilities, achieving 3.3 kg m^{-2} h^{-1} evaporation rate and 95% photothermal efficiency. The authors concluded that the

performance of these aerogels could potentially be further enhanced in flowing air, underscoring their effectiveness in desalinating natural seawater.

Ma et al.,[190] proposed an innovative columnar arrangement sodium alginate aerogel, incorporating sequentially organized MXene–carbon nanotubes and this design achieved a commendable evaporation rate of approximately 2.5 kg m^{-2} h^{-1}. The sodium alginate aerogel's hydrophilic nature enabled rapid water transport via capillary action through its directional channels, efficiently delivering water to the upper layer. By reducing the gap between vapor generation and escape locations, this design contributed to a significant enhancement in the system's capacity utilization efficiency. Cao et al.,[191] developed a photothermal membrane tailored for water treatment via interfacial evaporation. By integrating MXene surface functionalization with durable nonwoven fibre substrates, the evaporator exhibited maximum 1.5 kg m^{-2} h^{-1} evaporation rate under 1-sun using 10 cm^2 device area. This performance further improved, reaching an evaporation rate of 1.7 kg m^{-2} h^{-1} for a smaller-area device (4 cm^2). Jin et al.,[192] introduced a three-dimensional evaporator by combining carbon fibre, chitosan, and a MoS$_2$–MXene heterostructure. This innovative design resulted in an evaporator with remarkable mechanical strength and enhanced desalination capabilities. Under 1-sun, 2.5 kg m^2 h^{-1} evaporation rate of from bulk seawater was obtained,
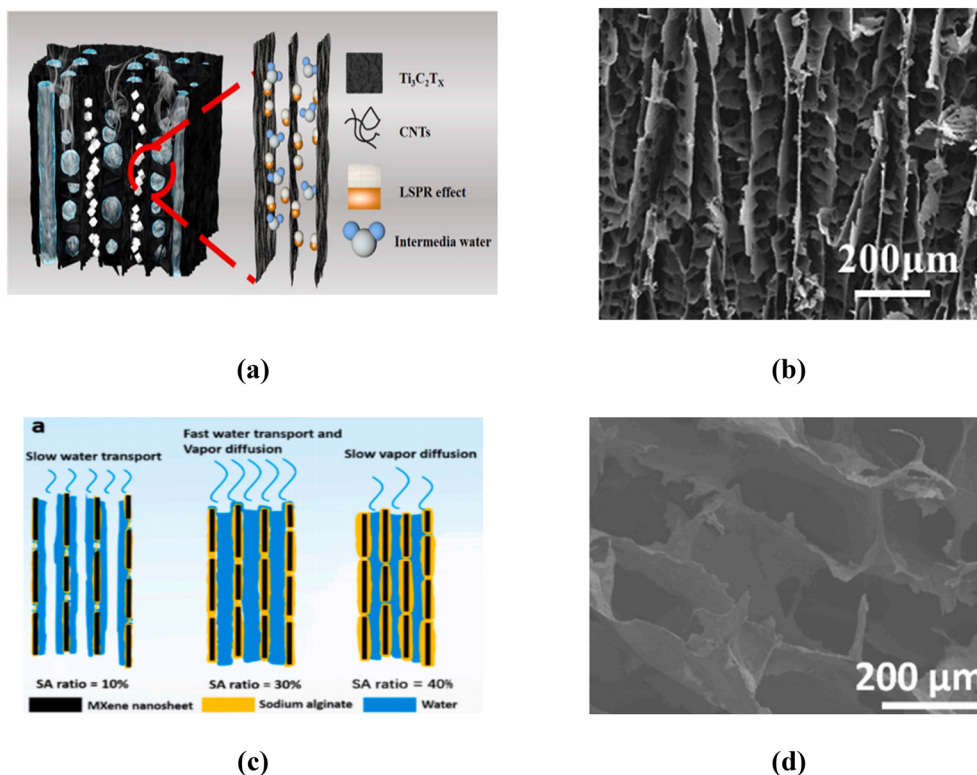

(a)

(b)

(c)

(d)

Fig. 12 (a) Schematic of the water evaporation mechanism in aerogels, (b) aerogel SEM image.[188] Reproduced from ref. 188 with permission from Elsevier, copyright 2024. (c) Schematic of water states around sodium alginate in MXene containing aerogel, (d) SEM image of the MXene–sodium alginate aerogel.[189] Reproduced from ref. 189 with permission from Elsevier, copyright 2024.

This journal is © The Royal Society of Chemistry 2025

Environ. Sci.: Nano, 2025, 12, 1012–1036 | 1029

approximately 20 times higher than under natural light conditions. The evaporation rates increased proportionally with higher irradiation, reaching 5.0 kg m^2 h^{-1} under 2.5-sun, as depicted in Fig. 13a, which illustrates the mass reduction and surface temperature changes under different levels of light intensity. The hydrophilicity of MoS_2, enhanced by MXene, facilitated continuous water pumping, while the excellent conductivity enabled operation even in low-light conditions. The evaporator sustained steady desalination performance over 20 hours in 3.5 wt% saline water and demonstrated strong salt resistance, even in high-salinity environments. Bai et al.[193] developed an evaporator by enhancing delignified coconut husks with diatomite and applying an MXene coating. The schematic of the stepwise fabrication process is presented in Fig. 13c. This innovative approach sought to enhance the evaporator's hydrophilicity by increasing the exposure of hydrophilic groups through

delignification, along with the incorporation of MXene and diatomite. The evaporator demonstrated a water 2 kg m^2 h^{-1} evaporation rate under 1-sun, showing greater performance compared to many devices reported in recent years (see Fig. 13c).

Wang et al.[194] fabricated Janus MXene–cellulose nanofiber–luffa aerogel with multifunctional properties, including rapid water transport, effective thermal management, swift vapor release, and efficient photothermal conversion. The aerogel's structure was meticulously designed, with the lower section measuring 9 mm and the upper section around 1 mm, facilitating water transport to the surface through strategically engineered water channels. The hydrophilic nature of the lower layer further supported water movement via capillary action, which is essential for consistent solar vapor generation. Water transport tests demonstrated that when the aerogel was placed on a hot
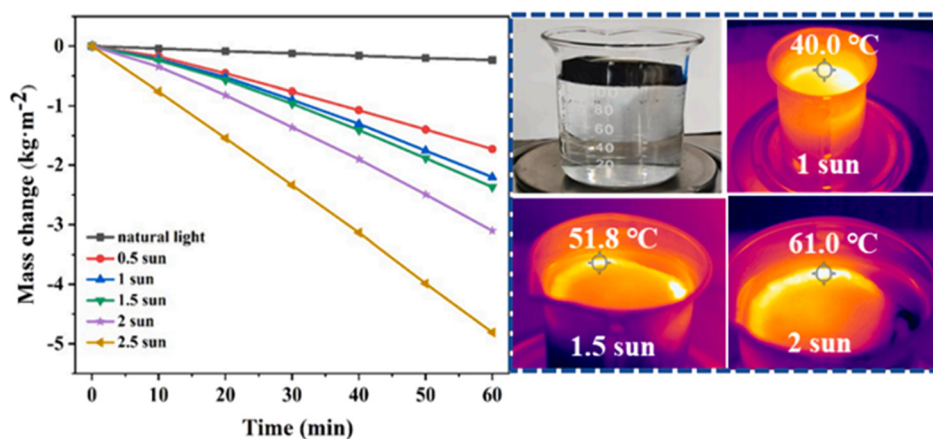
(a)
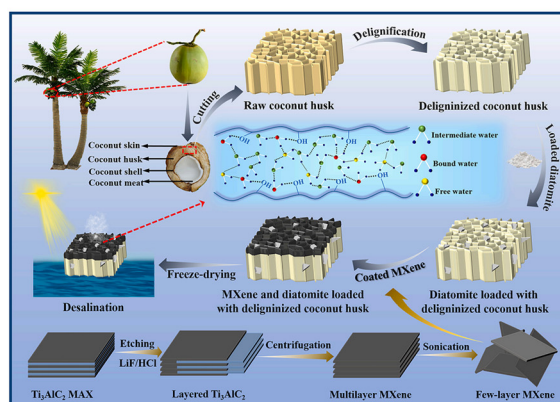
(b)
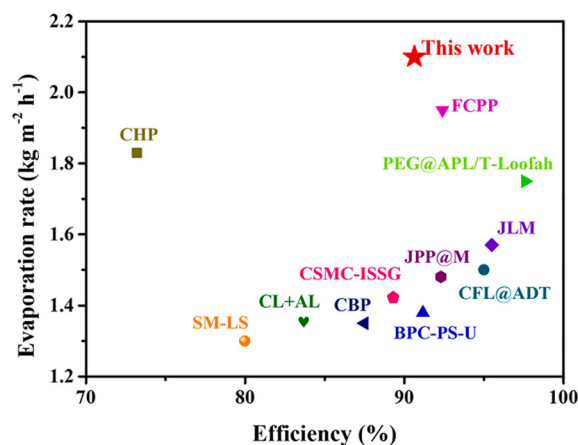
(c)

Fig. 13 (a) Evaporation rate *versus* time at different intensities with corresponding temperature rise.[192] Reproduced from ref. 192 with permission from Elsevier, copyright 2024. (b) Schematic of stepwise evaporator fabrication, (c) performance comparison of the desalination performance of the delignified coconut husks with diatomite and a MXene coating (indicated as * this work) with recent references.[193] Reproduced from ref. 193 with permission from Elsevier, copyright 2024.

1030 | *Environ. Sci.: Nano*, 2025, **12**, 1012–1036

This journal is © The Royal Society of Chemistry 2025

water surface ($\approx$40 °C), the temperature of the upper layer equalized within 30 seconds, signifying efficient water delivery to the photothermal layer. To optimize performance, the water paths were designed with symmetrical through-holes of 10 mm in diameter, balancing effective water transport while minimizing heat loss. Under 1-sun conditions, the aerogel achieved 1.40 kg m^2 h^{-1} evaporation rate. Hu et al.[195] developed porous wood-based solar steam generators, featuring a novel top-down water supply system designed to enhance evaporation efficiency. The fabrication process involved delignifying porous wood and impregnating it with polyvinyl alcohol and MXene. A key innovation of this system is the top-down water supply, which ensures continuous water delivery while mitigating salt deposition, thereby enhancing both evaporation efficiency and salt resistance. Under 1-sun, evaporator demonstrates evaporation rate of 4.3 kg m^2 h^{-1} and effectively desalinated a 15 wt% NaCl solution, maintaining this rate consistently. The exceptional evaporation efficiency and long-term stability are attributed to the synergy of the top-down water supply, MXene's highly efficient solar-thermal energy conversion, and the porous, hydrophilic characteristics of the delignified wood. Kröger et al.,[196] introduced an innovative MXene–aramid nanofiber composite film, fabricated using a straightforward vacuum filtration technique. This composite film exhibits impressive photothermal conversion capabilities and water evaporation performance. Furthermore, the film achieves a evaporation rate of 1.5 kg m^{-2} under solar irradiation at 1 kW m^{-2}, highlighting its potential for effective solar evaporation applications.

5. MXene for water purification and disinfection in hydroponics

As the demand for more sustainable and resource-efficient farming practices increases, hydroponic systems have emerged as a key solution for crop production, mainly in water-scarce regions. However, retaining water quality in these closed-loop systems is a major challenge, especially as the reuse of water can lead to the accumulation of contaminants, including heavy metals and pathogens. Recent advancements in MXene-based nanomaterials have unlocked new avenues for focusing these challenges. MXenes, are progressively recognized for their high surface area, ion selectivity, and antibacterial properties making them ideal candidates for incorporation into hydroponic water purification and disinfection systems.[197] MXenes exhibits a range of properties that are exceptionally helpful for filtering and removing harmful elements from nutrient solutions in hydroponic systems. These materials have shown strong ion selectivity and capacity for heavy metal removal through multiple methods such as ion exchange, electrostatic interactions, and complexation with surface functional groups. Some studies[198,199] reported the presence of heavy metals like nickel (Ni^{2+}), lead (Pb^{2+}), and cadmium (Cd^{2+}) for hydroponic production, which could be from contamination

from fertilizer sources. MXene membranes have been shown to effectively remove heavy metals like nickel (Ni^{2+}), lead (Pb^{2+}), and cadmium (Cd^{2+}),[198] which could accumulate in hydroponic production and can severely affect plant health as it could be easily absorbed by plants. By incorporating MXene-based membranes into hydroponic systems, it is possible to ensure that nutrient solutions remain free of these hazardous contaminants, facilitating better nutrient uptake and healthier plant growth. Also, MXenes filtration could be used for water purification for using wastewater for hydroponic applications. Moreover, MXenes are highly effective in water disinfection, owing to their potent antibacterial properties. These materials generate reactive oxygen species (ROS) and leverage their unique surface chemistry to disrupt bacterial membranes and prevent biofilm formation, making them highly effective against a range of waterborne pathogens. In hydroponic systems, risk of E. coli infection could be severe. A study conducted by Wang et al.,[200] revealed that Shiga toxin-producing E. coli (STEC) was present in hydroponic growing systems, although earlier assumptions that such systems could mitigate the risk of contamination. In both aquaponic and hydroponic systems, E. coli was found in the water, on plant roots, and even in the fish feces in aquaponic setups, posing a food safety concern. This contamination can lead to major health risks, specifically in leafy greens and other produce consumed raw. Thus, inhibiting E. coli from increasing in hydroponic systems is critical to ensuring end user safety and lowering the risk of foodborne illness. MXenes, specifically $Ti_3C_2T_x$, have showed strong antibacterial activity against Gram-negative bacteria like E. coli.[201] In water purification applications, MXene's capability to make ROS and damage bacterial cell membranes can be exceptionally effective in hydroponic systems where pathogens like E. coli may otherwise thrive. By incorporating MXene-based filtration into hydroponic setups, it may be possible to considerably lower the risk of E. coli contamination, offering a better, safer growing environment for crops. Another significant benefit of MXenes in hydroponic systems is their role in improving water recycling. MXene-based membranes can effectively filter organic and inorganic contaminants, supporting the reuse of water within the system and reducing the need for frequent water changes. This ability is predominantly crucial for the sustainability of hydroponic systems, as it reduces water wastage and improves resource efficiency, an extensive concern in water-scarce regions. Furthermore, MXene membranes show strong fouling resistance and enhanced durability, vital for long-term agricultural application. Though MXenes are still in the early stages of their application in water purification and agricultural science, their potential for improving hydroponic systems is obvious. Their multifunctionality extending from contaminant filtration to pathogen inhibition makes them critical for the future of sustainable farming. With continued research focused on refining the stability and scalability of MXenes for viable use, these materials could soon become

This journal is © The Royal Society of Chemistry 2025

Environ. Sci.: Nano, 2025, **12**, 1012–1036 | **1031**

standard in hydroponic water management systems, contribution a more effectual and ecologically friendly answer for food production.

6. Challenges

MXenes, a novel category of two-dimensional materials, present numerous benefits. Despite more than a decade of developmental research, MXene-based nanomaterials are still in the initial phases of advancement towards practical applications. To fully exploit their potential, standardization becomes crucial to attain enduring qualities like improved biocompatibility, consistent dispersion, extended durability, and enhanced productivity when compared to other two-dimensional materials. It is advisable to extensively employ MXene-based nanocomposite, membranes, adsorbents, and electrodes to facilitate efficient toxin removal. This approach will make cost-effective wastewater purification feasible for both residential and commercial purposes. However, there are some technical challenges that need to be overcome to realise this in practice, including:

i. Producing MXene films on a large-scale encounters two significant obstacles: oxidation and inadequate mechanical properties. Although annealing can alleviate oxidation, it remains a hindrance to commercial use. Additionally, weak interlayer interactions pose difficulties in obtaining self-supporting MXene films. To enable the large-scale manufacturing of MXenes (for example, using etching or drop cast method), it is crucial to enhance their environmental durability, mechanical resilience, and electrochemical characteristics.

ii. MXene composite membranes suffer from certain drawbacks, notably constrained permeation performance, low stability, and a limited lifespan. These limitations arise from the narrow interlayer spacing within the stacked structure, resulting in longer permeation paths and the accumulation, adsorption, and blockage of pores and the membrane's outer surface by pollutants in the feed streams. Nonetheless, enhancing permeance performance and resistance against swelling and fouling can be achieved through effective control of the structural interlayer channels. Techniques such as managing surface charge, incorporating companion materials between MXene layers, and utilizing nanoparticles to create pores show promising potential for controlling the membrane structure and enhancing its practical utility.

iii. The antibacterial and biofilm inhibitory properties of MXene can be classified into the following categories: induction by photothermal effect; generation of reactive oxygen species; modification of MXene surfaces. Therefore, MXenes exhibit promising potential in combating bacterial infection and addressing antibiotic resistance. The biocompatibility of MXene has not yet been fully investigated, although it is a crucial aspect of the therapeutic process. Some studies have suggested that MXenes may have cytotoxic effects on bacteria by disrupting the structure of lipid

bilayers. However, more research is needed to fully understand the mechanisms of cytotoxicity. Several MXene compositions have demonstrated biocompatibility, degradability, and rapid clearance from the body. Nevertheless, additional research is necessary to ascertain their biodistribution, pharmacological impact, and long-term toxicity, to fully understand the safety of MXenes for use in biomedical applications. Computational simulations can aid in comprehending the transformation of therapeutic agents and their potential side effects on healthy tissues.

iv. MXenes have exhibited promising antibacterial potential; however, there is a need for further research to fully uncover their capabilities and the mechanism of antimicrobial activity. For example, 2D graphene oxide (GO) materials have to show to exert different antimicrobial effects depending on their surface oxygen contents (SOC), switching from causing physical effects due to enwrapping bacterial cells to edge-on interactions leading to damage of the lipid membrane.[202] To optimize the antibacterial properties of MXenes, it is essential to examine the fundamental challenges related to factors such as their size, surface functionalization, and component mechanisms. Besides, MXenes demonstrate effectiveness in biomedical applications due to their distinctive combination of properties. MXenes are susceptible to environmental influences due to their extensive surface area, which limits their thermal stability. They decompose rapidly into oxides when exposed to air, moisture, and light. Therefore, ensuring the stability of MXenes is crucial in practical applications to guarantee their substantial antibacterial activity. Additionally, the oxidation of MXenes mainly occurs at the edges. Consequently, it may be worth investigating methods for passivating these sharp edges using impermeable materials and stable oxides.

v. MXenes have been employed to fabricate membranes for desalination and water treatment. Through precise adjustments to their surface chemistry, these membranes exhibit exceptional selectivity for ion separation, employing both size and charge sieving mechanisms, while also facilitating rapid water transport. The unique properties of MXenes render them suitable for voltage-gated ion transport, with potential applications in capacitive deionization. The interlayer spacing of stacked MXene sheets plays a crucial role in the membrane's separation efficiency, flow rate, and selectivity. However, in aqueous media, MXene membranes may undergo swelling, resulting in reduced ion rejection and selectivity. To tackle this issue, it is possible to regulate the channel size by fixing the interlayer spacing with intercalating and cross-linking molecules, preventing swelling and preserving the integrity of the 2D sheets.

vi. The variance in metallic and semiconductor behavior among MXene presents a challenge in exclusively attributing photothermal mechanisms to the LSPR effect, necessitating further inquiry. Moreover, the effective management of water supply and thermal balance by a solar-driven interfacial evaporation device is critical for overcoming this challenge in real-world conditions. Diversifying water sources to include

1032 | *Environ. Sci.: Nano*, 2025, **12**, 1012–1036

This journal is © The Royal Society of Chemistry 2025

wastewater with elevated salt levels or bacterial content is essential for extending interfacial steam generation beyond conventional desalination methods, facilitating its broader application across diverse fields.

vii. $Ti_3C_2T_x$ is extensively studied for water purification and environmental remediation and is commonly employed as an adsorbent for reductive metal ion removal and dye photodegradation. Nevertheless, compared to graphene and other 2D materials, $Ti_3C_2T_x$ has received relatively less exploration. Ti_2CT_x and Ti_3NC are promising alternatives with non-toxic decomposition products that warrant further attention. It is crucial to investigate new MXene structures that offer enhanced environmental stability, particularly for water-related applications. With over 30 MXenes predicted theoretically, there is the potential for a wider range of materials to become available for water treatment and other environmental applications.

7. Prospects and future recommendations

Since its invention, MXene has been extensively explored in various fields, including water purification and desalination systems; however, MXene-based materials including membranes for water treatment applications are still at an early stage of development. Hence, more research to overcome and address the remaining issues and challenges is needed. The current study complements the literature by detailing recent theoretical and practical breakthroughs in MXene for the above-mentioned applications. Based on the present review findings, we focus the attention of the reader on the following points:

i. Two-dimensional materials such as graphene, graphene oxide (GO), covalent frameworks (COFs), and metal–organic frameworks (MOFs), with unique atomic thickness, are promising candidates to be used as excellent membranes owing to their interesting characteristics such as large surface area, mechanical strength, stability, hydrophilic surface, and ease of functionalization. Evidence is mounting that MXene is an auspicious agent for next-generation separation technologies. This is attributed to their tunable physicochemical properties, in-plane pore structure, and inter-layer properties of 2D channels, making MXenes a better choice than other 2D materials for next-generation membranes.

ii. While membranes are generally very effective water purification tools, membrane fouling appears to be an inherent and unavoidable issue with membrane technology. Ongoing study on fouling behaviour is required to get a better knowledge of fouling mechanisms, which might give a stronger foundation for improving or re-developing fouling management techniques. While it appears complicated, innovative membrane materials and manufacturing procedures based on MXene and its combinations with other antifouling materials could provide a viable solution to the membrane fouling problem.

iii. Interfacial solar steam generation, a promising method for producing freshwater without pollution, faces significant obstacles in its widespread commercial adoption. The efficiency of freshwater production depends on the rates of evaporation and condensation collection. While evaporation rates can exceed theoretical expectations, the technology for collecting condensation often falls behind and is frequently neglected. The use of covers for collecting freshwater, essential for the process, presents difficulties as they reflect sunlight and may develop a liquid film, leading to increased heat loss, especially in conditions with high water vapor content.

iv. The structural properties of MXene have been thoroughly characterized to get a better knowledge of the optimal techniques for the synthesis of MXenes to be used in water purification and as desalination membranes. Even though MXene functionalization is frequently studied, investigations focusing on the adsorptive nature of MXenes without the attachment of functional groups are necessary to enable new insights and further optimization of separation capability and reduced biofouling.

v. Assessment of MXene's toxicity should be prioritized for use in water purification and desalination. MXene toxicity is affected by its functional groups and size, oxidative state (Ti_2O_3), manufacturing techniques, type and administration dosage, and exposure periods (24–48 h). More efforts are required to design safe MXenes (safe-by-design) by control and optimization of operating circumstances and assessment of particle release during extended use cycles under the actual use conditions (*e.g.*, high salt, high temperature, potentially NIR light *etc.*) and at end of life, following disposal. Consideration of the potential for easy re-generation of MXene-containing membranes and/or recycling of critical elements should be considered prior to mass production and commercialization.

vi. Machine learning and artificial intelligence approaches might help to advance the field of water filtration and desalination, as well as create methodologies to anticipate the toxicity of experimentally generated MXenes, and indeed to feed into the safe-by-design optimization of MXenes for environmental applications. These methods may minimize the quantity of toxicity investigations needed.

Finally, to enhance separation performance, controlled physicochemical characteristics of MXenes and the operating conditions should be optimized. In the field of water purification and desalination, MXene is considered a novel material and is at an early stage of development. Thus, we highly recommend scientists to focus on understanding MXene as a material, and its separation properties, to optimize its separation and water permeability performances. Further research is needed to develop high performance and durable membranes, considering the membrane's interlayer spacing and their fouling resistance and antibacterial activity. Another factor to consider when using MXene as a desalination-based material is that MXene is easily oxidized in the presence of water and oxygen. As a result, it is strongly

This journal is © The Royal Society of Chemistry 2025

Environ. Sci.: Nano, 2025, **12**, 1012–1036 | 1033

advised to work on enhancing MXenes' stability, hydrophobic characteristics, and chemical functions. Furthermore, upgrading MXene-based membrane structure by incorporating a hierarchical crumpled structure, microporous structure, and Janus structure may increase water transport and hence reduce MXene oxidation.

Data availability

No primary research results, software or code have been included and no new data were generated or analysed as part of this review.

Conflicts of interest

The authors declare that they have no conflicts of interest.

Acknowledgements

References

1   Y. Liang, *et al.*, *Energy Convers. Manage.*, 2022, **266**, 115740.
2   S. Sarathe, *et al.*, *Mater. Today: Proc.*, 2022, **56**, 326–335.
3   D. Song, *et al.*, *Energy Convers. Manage.*, 2022, **260**, 115576.
4   J. Koschikowski, M. Wieghaus and M. Rommel, *Desalination*, 2003, **156**, 295–304.
5   E. Gontarek-Castro, G. Di Luca, M. Lieder and A. Gugliuzza, *Membranes*, 2022, **12**(5), 511.
6   Z. Mahmood, H. Cheng and M. Tian, *Environ. Sci.: Water Res. Technol.*, 2022, **8**(10), 2126–2144.
7   F. H. Memon, *et al.*, *Sep. Purif. Rev.*, 2023, **52**, 43–57.
8   A. Matin, *et al.*, *Sci. Total Environ.*, 2021, **765**, 142721.
9   S. Goh, *et al.*, *Desalination*, 2018, **425**, 130–155.
10   S. Yang, *et al.*, *J. Mol. Liq.*, 2022, **349**, 118115.
11   Y. Cao, *et al.*, *Eur. Phys. J. Plus*, 2022, **137**(7), 763.
12   A. Selvam, *et al.*, *Sol. RRL*, 2022, **6**(8), 2200321.
13   R. Ahmadi, *et al.*, *J. Appl. Polym. Sci.*, 2022, **139**(22), 52262.
14   Y. Wen, *et al.*, *Sci. Adv.*, 2022, **8**(10), 4149.
15   T. Zhang, *et al.*, *Desalination*, 2022, **527**, 115576.
16   H. Meskher, *et al.*, in *Age of MXenes, Volume 2. Applications in Diagnostics, Therapeutics, and Environmental Remediation*, 2023, ch. 4, pp. 61–83.
17   L. Zhao and B. Li, *Tungsten*, 2020, **2**, 176–193.
18   M. Berkani, *et al.*, *Environ. Res.*, 2022, **203**, 111845.
19   C. Lamiel, *et al.*, *Mater. Today*, 2023, **63**, 313–338.
20   A. Thakur, *et al.*, *Small Methods*, 2023, **7**(8), 2300030.
21   F. Dixit, *et al.*, *J. Hazard. Mater.*, 2022, **423**, 127050.
22   A. Qureshi and A. H. Abdelhay, *et al.*, *Crit. Rev. Solid State Mater. Sci.*, 2024, **49**(1), 141–162.
23   S. He, *et al.*, *Adv. Mater. Technol.*, 2022, **7**(7), 2101343.
24   L. Ding, *et al.*, *Nat. Sustain.*, 2020, **3**(4), 296–302.
25   S. Zhang, *et al.*, *Chemosphere*, 2021, **283**, 131293.
26   N. Sheikh, *et al.*, *Int. J. Energy Res.*, 2021, **45**(12), 17563–17576.
27   S. Wang, *et al.*, *Chem. Soc. Rev.*, 2020, **49**(4), 1071–1089.
28   O. Kwon, *et al.*, *Desalination*, 2022, **522**(115448), 2022.
29   A. Isfahani and A. Arabi Shamsabadi, *et al.*, *Ind. Eng. Chem. Res.*, 2023, **62**(5), 2309–2328.
30   Y. Wei, *et al.*, *Adv. Mater.*, 2021, **33**(39), 2103148.
31   Z. Huang, *et al.*, *J. Membr. Sci.*, 2021, **640**, 119854.
32   Y. Mansourpanah, *Sep. Purif. Technol.*, 2022, **289**, 120777.
33   X. Wu, *et al.*, *ACS Nano*, 2020, **14**(7), 9125–9135.
34   X. Feng, *et al.*, *Sep. Purif. Technol.*, 2020, **247**, 116945.
35   J. A. Kumar, *et al.*, *Chemosphere*, 2022, **286**, 131607.
36   X. Wang, Q. Li, J. Zhang, H. Huang, S. Wu and Y. Yang, *J. Membr. Sci.*, 2020, **603**, 118036.
37   T. Bashir, S. Zhou and S. Yang, *et al.*, *Electrochem. Energy Rev.*, 2023, **6**, 5.
38   Z. Zhao, Y. Song and X. Liu, *et al.*, *J. Energy Storage*, 2024, **86**, 111253.
39   A. C. Ezika, E. R. Sadiku, S. S. Ray, Y. Hamam and G. J. Adekoya, *S. Afr. J. Chem. Eng.*, 2023, **44**, 297–301.
40   G. Saeed, A. Alam and S. Bo, *et al.*, *Chem. Eng. J.*, 2023, **477**, 146995.
41   C. Xu, L. Tong, W. Zhang, X. Zhao, L. Yang and S. Yin, *Chem. Eng. J.*, 2024, **497**, 154449.
42   K. Teenakul, S. A. Ahmad Alem, R. Gond, A. Thakur, B. Anasori and A. Khataee, *RSC Adv.*, 2024, **14**, 12807–12816.
43   L. Jiang, *et al.*, *J. Mater. Chem. A*, 2022, **10**(26), 13651–13672.
44   X. Ma, *et al.*, *J. Membr. Sci.*, 2022, **647**, 120334.
45   L. Ding, *et al.*, *Angew. Chem., Int. Ed.*, 2017, **56**(7), 1825–1829.

1034 | *Environ. Sci.: Nano*, 2025, **12**, 1012–1036

This journal is © The Royal Society of Chemistry 2025

46 S. Zhang, *et al.*, *Adv. Mater.*, 2022, **34**(21), 2108457.
47 T. Zhang, *et al.*, *J. Membr. Sci.*, 2022, **641**, 119907.
48 G. Lim, *et al.*, *Ceram. Int.*, 2022, **48**, 16477–16491.
49 Y. Li, *et al.*, *J. Cleaner Prod.*, 2022, **347**, 131324.
50 I. Ihsanullah, *et al.*, *Chemosphere*, 2022, **303**, 135234.
51 Q. Long, *et al.*, *J. Membr. Sci.*, 2021, **635**, 119464.
52 B. Meng, *et al.*, *J. Membr. Sci.*, 2021, **623**, 119076.
53 Y. A. J. Al-Hamadani, *et al.*, *Chemosphere*, 2020, **254**, 126821.
54 K. R. G. Lim, *et al.*, *Nat. Synth.*, 2022, **1**(8), 601–614.
55 S. Zhang, *et al.*, *J. Hazard. Mater.*, 2020, **384**, 121367.
56 P. Zhou, *et al.*, *Chem. Eng. J.*, 2023, **464**, 142508.
57 K. Zarshenas, *et al.*, *ACS Appl. Mater. Interfaces*, 2022, **14**(1), 1838–1849.
58 Z. Liao, *et al.*, *Sep. Purif. Technol.*, 2021, **266**, 118567.
59 T. Zhang, *et al.*, *Water Res.*, 2022, **216**, 118349.
60 Y. Wu, *et al.*, *Chem. Eng. J.*, 2021, **418**, 129296.
61 S. Yu, *et al.*, *Sci. Total Environ.*, 2022, **811**, 152280.
62 S. Siddique, *et al.*, *Prog. Mater. Sci.*, 2023, **139**, 101183.
63 Y. Zhang, *et al.*, *ACS Appl. Mater. Interfaces*, 2019, **11**(50), 47350–47357.
64 H. Assad, *et al.*, *Chemosphere*, 2022, **298**, 134221.
65 A. Zamhuri, *et al.*, *Biomed. Eng. Online*, 2021, **20**(1), 33.
66 T. Liu, *et al.*, *J. Membr. Sci.*, 2020, **593**, 117431.
67 J. Wang, *et al.*, *Nanoscale*, 2017, **9**(9), 2942–2957.
68 X. Zhao, *et al.*, *Adv. Mater. Interfaces*, 2022, **9**(20), 2200480.
69 T. Li, *et al.*, *Angew. Chem., Int. Ed.*, 2018, **57**(21), 6115–6119.
70 H. Shi, *et al.*, *Angew. Chem., Int. Ed.*, 2021, **60**(16), 8689–8693.
71 Y. Li, *et al.*, *Nat. Mater.*, 2020, **19**(8), 894–899.
72 F. Shahzad, *et al.*, *Adv. Mater.*, 2020, **32**(51), 2002159.
73 B. C. Wyatt, *et al.*, *Adv. Mater.*, 2021, **33**(17), 2007973.
74 X. Zhan, *et al.*, *Nanoscale Horiz.*, 2020, **5**(2), 235–258.
75 Y. Zhang, *et al.*, *ACS Appl. Mater. Interfaces*, 2019, **11**, 47350–47357.
76 E. Ghasali, *et al.*, *Appl. Surf. Sci.*, 2021, **542**, 148538.
77 J. Zhao, *et al.*, *Dalton Trans.*, 2019, **48**, 14433–14439.
78 F. Turker, *et al.*, *J. Am. Ceram. Soc.*, 2020, **103**, 5586–5593.
79 A. L. Lehninger, *Physiol. Rev.*, 1950, **30**, 393–429.
80 P. Srivastava, *et al.*, *ACS Appl. Mater. Interfaces*, 2016, **8**, 24256–24264.
81 M. Shen, *et al.*, *Angew. Chem.*, 2021, **133**, 27219–27224.
82 Y. Yang, *et al.*, *Nanoscale*, 2019, **11**, 16–33.
83 S. Zhang, *Nat. Biotechnol.*, 2003, **21**, 1171–1178.
84 K. T. Young, *et al.*, *J. Vac. Sci. Technol., A*, 2021, **39**, 012201.
85 Z. Zhang, *et al.*, *Nano Lett.*, 2019, **19**, 3327–3335.
86 L. Jiang, *et al.*, *J. Mater. Chem. A*, 2022, **10**, 13651–13672.
87 A. Sohan, *et al.*, *Int. J. Energy Res.*, 2021, **45**, 19746–19771.
88 Y. A. J. Al-Hamadani, *et al.*, *Chemosphere*, 2020, **254**, 126821.
89 X. Liu, *et al.*, *J. Membr. Sci.*, 2022, **654**, 120469.
90 J. A. L. Willcox, *et al.*, *ACS Nano*, 2017, **11**(2), 2187–2193.
91 R. R. Nair, *et al.*, *Science*, 2012, **335**(6067), 442–444.
92 Z. Qin, *et al.*, *RSC Adv.*, 2017, **7**(85), 54213–54221.
93 O. O. Compton, *et al.*, *ACS Nano*, 2012, **6**(3), 2008–2019.
94 Z. Lu, *et al.*, *ACS Nano*, 2019, **13**(9), 10535–10544.
95 Y. Han, *et al.*, *Adv. Funct. Mater.*, 2013, **23**(29), 3693–3700.
96 R. Han, *et al.*, *J. Mater. Chem. A*, 2019, **7**(11), 6475–6481.
97 M. Shahat, *Acta Crystallogr.*, 1952, **5**(6), 763–768.
98 I. Ihsanullah, *Nano-Micro Lett.*, 2020, **12**(1), 72.
99 Q. Zhang, *et al.*, *ACS Nano*, 2019, **13**(11), 13196–13207.
100 K. A. Mahmoud, *et al.*, *Desalination*, 2015, **356**, 208–225.
101 M. F. El-Kady, *et al.*, *Nat. Rev. Mater.*, 2016, **1**(7), 16033.
102 F. Rehman, *et al.*, *Rev. Inorg. Chem.*, 2022, **42**, 0035.
103 F. Rehman, *et al.*, in *Nanotechnology in the Beverage Industry, Fundamentals and Applications*, Elsevier, 2020, pp. 207–240.
104 S. K. Raj, *et al.*, in *2D Nanomaterials for Energy and Environmental Sustainability*, Springer Nature Singapore, 2022, pp. 125–148.
105 Y. Z. Tan, *et al.*, *J. Membr. Sci.*, 2018, **565**, 254–265.
106 R. Han, *et al.*, *RSC Adv.*, 2017, **7**, 56204–56210.
107 L. Ding, *et al.*, *Nat. Sustain.*, 2020, **3**, 296–302.
108 J. Deng, Z. Lu and L. Ding, *et al.*, *Chem. Eng. J.*, 2021, **408**, 127806.
109 Z. Lu, *et al.*, *ACS Nano*, 2019, **13**, 10535–10544.
110 K. M. Kang, D. W. Kim and C. E. Ren, *et al.*, *ACS Appl. Mater. Interfaces*, 2017, **9**, 44687–44694.
111 R. Han and P. Wu, *J. Mater. Chem. A*, 2019, **7**(11), 6475–6481.
112 Z. Lu, *et al.*, *Angew. Chem.*, 2021, **133**, 22439–22443.
113 Q. Xue and K. Zhang, *J. Membr. Sci.*, 2021, **640**, 119808.
114 Y. Sun, D. Xu and S. Li, *et al.*, *J. Membr. Sci.*, 2021, **623**, 119075.
115 B. Meng, *et al.*, *J. Membr. Sci.*, 2021, **623**, 119076.
116 X. Zhu, X. Zhang and J. Li, *et al.*, *J. Membr. Sci.*, 2021, **635**, 119536.
117 M. Mustakeem, *et al.*, *ACS Appl. Mater. Interfaces*, 2022, **14**, 5265–5274.
118 Y. Sun, *et al.*, *J. Membr. Sci.*, 2019, **591**, 117350.
119 R. P. Pandey, *et al.*, *J. Mater. Chem. A*, 2018, **6**, 3522–3533.
120 M. A. Zaed, *et al.*, *Sep. Purif. Technol.*, 2025, **354**, 129055.
121 I. Ihsanullah, *Chem. Eng. J.*, 2020, **388**, 124340.
122 M. Mozafari, *et al.*, *Adv. Mater. Technol.*, 2021, **6**(10), 2001189.
123 C. E. Ren, *et al.*, *J. Phys. Chem. Lett.*, 2015, **6**(20), 4026–4031.
124 K. M. Kang, *et al.*, *ACS Appl. Mater. Interfaces*, 2017, **9**(51), 44687–44694.
125 T. Liu, *et al.*, *J. Membr. Sci.*, 2020, **593**, 117431.
126 J. Wang, *et al.*, *Nat. Commun.*, 2020, **11**(1), 3540.
127 H. Liu, *et al.*, *Nanoscale*, 2022, **14**(26), 9218–9247.
128 Z. Huang, *et al.*, *J. Membr. Sci.*, 2021, **623**, 119080.
129 W. Tian, *et al.*, *Nat. Commun.*, 2019, **10**, 2558.
130 M. Homocianu, *et al.*, *J. Environ. Manage.*, 2022, **311**, 114817.
131 X. Liu, *et al.*, *Water Cycle*, 2021, **2**, 51–63.
132 H. Chen, *et al.*, *Sci. Total Environ.*, 2020, **739**, 139944.
133 S. Jiang, *et al.*, *Sci. Total Environ.*, 2017, **595**, 567–583.
134 R. Pandey, *et al.*, *J. Mater. Chem. A*, 2018, **6**(8), 3522–3533.
135 R. Han, *et al.*, *Chin. J. Chem. Eng.*, 2019, **27**(4), 877–883.
136 I. Mahar, *et al.*, *Membranes*, 2021, **11**(11), 869.
137 Z. Shen, *et al.*, *Int. J. Environ. Res. Public Health*, 2019, **16**(23), 4659.

This journal is © The Royal Society of Chemistry 2025

Environ. Sci.: Nano, 2025, **12**, 1012–1036 | 1035

138 C. Wang, *et al.*, *ACS Appl. Mater. Interfaces*, 2020, **12**, 43032–43041.

139 L. Zhang, *et al.*, *Water Res.*, 2022, **219**, 118598.

140 B. Meng, *et al.*, *J. Membr. Sci.*, 2021, **623**, 119076.

141 X. R. Wang, *et al.*, *ACS Appl. Mater. Interfaces*, 2022, **14**, 53150–53164.

142 H. Chen, *et al.*, *ACS Appl. Electron. Mater.*, 2021, **3**, 4509–4516.

143 J. Li, *et al.*, *ACS Appl. Nano Mater.*, 2022, **5**, 7373–7381.

144 Q. Feng, *et al.*, *Sep. Purif. Technol.*, 2022, **298**, 121635.

145 C. E. Shuck, *et al.*, *ACS Chem. Health Saf.*, 2021, **28**, 326–338.

146 M. V. D. Z. Park, *et al.*, *ACS Nano*, 2017, **11**, 9574–9593.

147 Y. Fan, *et al.*, *Chem. Eng. J.*, 2020, **401**, 126073.

148 C. E. Ren, *et al.*, *ACS Appl. Nano Mater.*, 2018, **1**, 3644–3652.

149 Y. Wang, *et al.*, *ACS Nano*, 2019, **13**, 11793–11799.

150 A. Siddiqua, *et al.*, *Environ. Sci. Pollut. Res.*, 2022, **29**(39), 58514–58536.

151 J. Stec, *et al.*, *Int. J. Environ. Res. Public Health*, 2022, **19**(12), 7308.

152 U. Qumar, *et al.*, *Nanotechnology*, 2021, **32**(15), 255704.

153 A. Raza, *et al.*, *Appl. Nanosci.*, 2020, **10**(10), 3875–3899.

154 S. Zhu, *et al.*, *Adv. Drug Delivery Rev.*, 2022, **188**, 114420.

155 Q. Feng, *et al.*, *Sep. Purif. Technol.*, 2022, **298**, 121635.

156 T. Zhang and L. Z. Zhang, *Water Res.*, 2022, **216**, 118349.

157 R. Alfahel, *et al.*, *J. Water Process Eng.*, 2020, **38**, 101551.

158 K. Rasool, *et al.*, *Sci. Rep.*, 2017, **7**(1), 1598.

159 E. A. Mayerberger, *et al.*, *RSC Adv.*, 2018, **8**(62), 35386–35394.

160 A. Rozmysłowska-Wojciechowska, *et al.*, *RSC Adv.*, 2019, **9**(8), 4092–4105.

161 A. M. Jastrzębska, *et al.*, *J. Mater. Eng. Perform.*, 2019, **28**(3), 1272–1277.

162 X. Zhu, *et al.*, *Nanoscale*, 2020, **12**(37), 19129–19141.

163 M. N. A. S. Ivan, *et al.*, *Nano Energy*, 2024, **120**, 109176.

164 B. Yu, *et al.*, *Adv. Funct. Mater.*, 2023, **33**, 2307533.

165 D. Xu, *et al.*, *Adv. Funct. Mater.*, 2020, **30**, 2000712.

166 R. Li, *et al.*, *ACS Nano*, 2017, **11**, 3752–3759.

167 H. Lin, *et al.*, *Nano Lett.*, 2017, **17**, 384–391.

168 X. Fan, *et al.*, *J. Mater. Chem. A*, 2019, **7**, 14319–14327.

169 K. Chaudhuri, *et al.*, *ACS Photonics*, 2018, **5**, 1115–1122.

170 F. Shahzad, *et al.*, *Science*, 2016, **353**(6304), 1137–1140.

171 K. Li, *et al.*, *Adv. Energy Mater.*, 2019, **9**, 1901687.

172 C. Cai, *et al.*, *Sol. RRL*, 2021, **5**, 2100593.

173 H. Li, *et al.*, *ACS Appl. Nano Mater.*, 2021, **4**, 14274–14284.

174 Z. Yang, *et al.*, *J. Colloid Interface Sci.*, 2024, **656**, 189–199.

175 A. M. Saleque, *et al.*, *Desalination*, 2023, **554**, 116488.

176 M. N. A. S. Ivan, *et al.*, *J. Mater. Chem. A*, 2023, **11**, 3961–3974.

177 Q. Zhang, *ACS Nano*, 2019, **13**, 13196–13207.

178 X. J. Zha, *et al.*, *ACS Appl. Mater. Interfaces*, 2019, **11**, 36589–36597.

179 Y. Bai, *et al.*, *J. Environ. Chem. Eng.*, 2024, **12**, 112282.

180 X. Fan, *et al.*, *Chem. Eng. J.*, 2024, **483**, 149304.

181 M. Sun, *et al.*, *Desalination*, 2023, **555**, 116462.

182 X. Fan, *et al.*, *Adv. Funct. Mater.*, 2020, **30**, 2007110.

183 Y. Yang, *et al.*, *J. Mater. Chem. A*, 2021, **9**, 23968–23976.

184 Z. Lei, *et al.*, *Nano-Micro Lett.*, 2022, **14**, 10.

185 L. Li, *et al.*, *Adv. Funct. Mater.*, 2021, **31**, 2104380.

186 J. Su, *et al.*, *Desalination*, 2023, **566**, 116905.

187 Y. Li, *et al.*, *J. Cleaner Prod.*, 2022, **347**, 131324.

188 J. Wu, D. Liu and Y. Sun, *et al.*, *Carbon*, 2024, **223**, 118976.

189 Y. Zhang, S. Wang and D. Han, *et al.*, *Desalination*, 2024, **585**, 117772.

190 X. Ma, N. Tian, G. Wang, W. Wang, J. Miao and T. Fan, *Desalination*, 2023, **550**, 116397.

191 Y. Cao, Y. Wang and J. Nie, *et al.*, *J. Colloid Interface Sci.*, 2024, **671**, 553–563.

192 L. Jin, *et al.*, *Chem. Eng. J.*, 2024, **497**, 154469.

193 Y. Bai, Y. Gu, J. Chen and Y. Yue, *J. Environ. Chem. Eng.*, 2024, **12**, 112282.

194 P. L. Wang, *et al.*, *J. Colloid Interface Sci.*, 2023, **645**, 306–318.

195 C. Hu, W. Li and H. Y. Zhao, *et al.*, *Chem. Eng. J.*, 2023, **460**, 141622.

196 H. Kröger, I. Donner and G. Skiello, *Arzneimittelforschung*, 1975, **25**, 1426–1429.

197 A. Mosa, *et al.*, *Chemosphere*, 2016, **146**, 30–37.

198 Á. Csog, *et al.*, *J. Plant Physiol.*, 2011, **168**(10), 1038–1044.

199 M. G. Cannata, *et al.*, *Commun. Soil Sci. Plant Anal.*, 2013, **44**(5), 952–961.

200 Y. J. Wang, A. J. Deering and H. J. Kim, *Horticulturae*, 2020, **6**(1), 1.

201 K. Rasool, *et al.*, *ACS Nano*, 2016, **10**(3), 3674–3684.

202 Z. Guo, *et al.*, *ACS Nano*, 2023, **17**, 6350–6361.

1036 | *Environ. Sci.: Nano*, 2025, **12**, 1012–1036

This journal is © The Royal Society of Chemistry 2025